Supporting Online Material for

Designed Synthesis of 3D Covalent Organic Frameworks

Hani M. El-Kaderi, Joseph R. Hunt, José L. Mendoza-Cortés, Adrien P. Côté,
Robert E. Taylor, Michael O'Keeffe, Omar M. Yaghi*

*To whom correspondence should be addressed. E-mail: yaghi@chem.ucla.edu

This PDF file includes:

Materials and Methods
Figs. S1 to S56
Tables S1 to S6
References

Materials and Methods for
Designed Synthesis of 3-D Covalent Organic Frameworks

Hani M. El-Kaderi[1], Joseph R. Hunt[1], José L. Mendoza-Cortés[1], Adrien P. Côté[1],
Robert E. Taylor[1], Michael O'Keeffe[2], Omar M. Yaghi[1]*

[1]Center for Reticular Chemistry at California NANOSystems Institute, Department of
Chemistry and Biochemistry, University of California, Los Angeles, 607 Charles E.
Young Drive East, Los Angeles, California 90095, USA. [2]Department of Chemistry and
Biochemistry, Arizona State University, Tempe, Arizona 85287, USA.

*To whom correspondence should be addressed. E-Mail: yaghi@chem.ucla.edu

Materials and Methods Table of Contents

Materials and Methods Section S1: *3-D COF Structural Models and Calculation of Simulated PXRD patterns.*

***Cerius²* Modeling** (development of synthetic blueprint for 3-D COFs).

All models were generated using the *Cerius²* chemical structure-modeling software suite (*1*) employing the crystal building module. Carbon nitride structures were created by starting with the space group $I\bar{4}3d$, cell dimensions and vertex positions obtained from the Reticular Chemistry Structure Resource (http://okeeffe-ws1.la.asu.edu/RCSR/home.htm) under the symbol **ctn** (*2*). The model of COF-102 was built from **ctn** by replacing the nitrogen (3-coordinate node) with the B_3O_3 (boroxine) unit positioning boron at each vertex of the triangle. Then the C-N bond in the structure was replaced by phenyl rings and the piecewise constructed structure was minimized using Universal Force Field (UFF) of *Cerius²* (*3*). The model of COF-103 was created using the method described above except carbon was substituted with silicon. Likewise, COF-105 was built in a similar fashion to COF-103 except the 3-coordinate species was substituted by 2,3,6,7,10,11-hexadydroxytriphenylene (HHTP) with the boron of the triboronate ester defining the vertex of the triangular unit.

Boracite structures were created starting with the space group $P\bar{4}3m$, cell dimensions and vertex positions obtained from the Reticular Chemistry Structure Resource (http://okeeffe-ws1.la.asu.edu/RCSR/home.htm) under the symbol **bor** (*2*). The model of COF-108 was created using the method described above except the B_3O_3 (boroxine) unit was replaced by the HHTP with the boron of the triboronate ester in each vertex of the triangle.

Positions of atoms in the respective unit cells are listed as fractional coordinates in Tables S1-S4. Simulated PXRD patterns were calculated from these coordinates using the PowderCell program (*4*). This software accounts for both the positions and types of atoms in the structures and outputs correlated PXRD patterns whose line intensities reflect the atom types and positions in the unit cells.

Table S1: Fractional atomic coordinates for COF-102 calculated from *Cerius²* modeling.

COF-102			
Space group symmetry $I\bar{4}3d$ $a = b = c = 27.1771\ (13)\ \text{Å}$ $\alpha = \beta = \gamma = 90°$			
Atom	x	y	z
O1	0.8285	0.74693	0.30298
B1	0.83533	0.71325	0.26216
C1	0.9049	0.76629	0.22758
C2	0.87894	0.72231	0.2263
C3	0.9312	0.69419	0.16049
C4	0.95634	0.7393	0.1596
C5	0.89252	0.6863	0.19272
C6	0.94306	0.77459	0.19484
C7	1.0	0.75	0.125
H1	0.89552	0.7946	0.25352
H2	0.94125	0.66415	0.13717
H3	0.87377	0.6515	0.19176
H4	0.96223	0.80911	0.1966

Table S2: Fractional atomic coordinates for COF-103 calculated from *Cerius^2* modeling.

COF-103			
Space group symmetry $I\bar{4}3d$ $a = b = c = 28.2477\ (21)$ Å $\alpha = \beta = \gamma = 90º$			
Atom	x	y	z
O1	0.20173	0.17738	0.24979
B1	0.24102	0.17052	0.21731
C1	0.3407	0.07966	0.20001
C2	0.33591	0.05139	0.24007
C3	0.30021	0.06125	0.27253
C4	0.26989	0.09921	0.26533
C5	0.27496	0.12788	0.22549
C6	0.31062	0.11783	0.1929
Si1	0.375	0.0	0.25
H1	0.36748	0.07242	0.17407
H2	0.29575	0.03949	0.30345
H3	0.24263	0.10607	0.291
H4	0.31517	0.1392	0.16171

Table S3: Fractional atomic coordinates for COF-105 calculated from *Cerius²* modeling.

COF-105			
Space group symmetry $I\bar{4}3d$ $a = b = c = 44.886\ (5)\ \text{Å}$ $\alpha = \beta = \gamma = 90°$			
Atom	x	y	z
O1	0.24923	0.26434	0.11672
O2	0.12931	0.20284	0.29149
B1	0.28905	0.10906	0.22877
C1	0.22645	0.21781	0.18335
C2	0.20018	0.23477	0.19174
C3	0.23455	0.25261	0.14166
C4	0.20882	0.26778	0.14873
C5	0.19137	0.25958	0.17328
C6	0.24387	0.22787	0.15826
C7	0.35228	0.05035	0.21728
C8	0.34987	0.03288	0.24348
C9	0.32755	0.03978	0.26475
C10	0.30811	0.0641	0.26008
C11	0.31075	0.0818	0.23403
C12	0.33294	0.07478	0.21265
Si1	0.375	0.0	0.25
H1	0.17131	0.2727	0.1768
H2	0.26464	0.21763	0.15114
H3	0.36894	0.04522	0.20028
H4	0.33529	0.08803	0.19228
H5	0.32518	0.02632	0.28497
H6	0.29108	0.06904	0.27686

Table S4: Fractional atomic coordinates for COF-108 calculated from *Cerius²* modeling.

COF-108			
Space group symmetry $P\bar{4}3m$ $a = b = c = 28.401\ (5)\ \text{Å}$ $\alpha = \beta = \gamma = 90°$			
Atom	*x*	*y*	*Z*
O1	0.67143	0.85456	0.08457
B1	0.64886	0.89710	0.10290
C1	0.60702	0.92264	0.07736
C2	0.53295	0.97038	0.02962
C3	0.77691	0.81243	0.15180
C4	0.58884	0.96472	0.09527
C5	0.55309	0.98865	0.07139
C6	0.77691	0.84820	0.18757
C7	0.70726	0.88278	0.15107
C8	0.74101	0.88337	0.18627
C9	0.500	0.00	0.000
H1	0.60305	0.87282	0.02007
H2	0.54196	0.91468	-0.02225
H3	0.73800	0.91161	0.21118

Note : Since the identity and number of guests is not known for COF-108 the structure was refined with no guests included in the model and this pattern is shown in Figures S8. Despite this the refinement gave very good r factors and a good fitting indicating that the proposed structure is correct. However for Figure 2D in the paper a calculated pattern is shown that contains one carbon atom in the center of the structure at 0.5 0.5 0.5 a,b,c to represent guests that may still be in the structure.

Materials and Methods Section S2*: X-ray Data Collection, Unit Cell Determination, and*

Le Bail Extraction. Powder X-ray data were collected using a Bruker D8-Discover θ-2θ diffractometer in reflectance Bragg-Brentano geometry employing Ni filtered Cu Kα line focused radiation at 1600 W (40 kV, 40 mA) power and equipped with a Vantec Line detector. Radiation was focused using parallel focusing Gobel mirrors. The system was also outfitted with an anti-scattering shield which prevents incident diffuse radiation from hitting the detector, preventing the normally observed large background at 2θ < 3º. Samples were mounted on zero background sample holders by dropping powders from a wide-blade spatula and then leveling the sample surface with a razor blade. Given that the particle size of the 'as synthesized' samples were already found to be quite mono-disperse no sample grinding or sieving was used prior to analysis, we note, however, that the micron sized crystallites lead to peak broadening. The best counting statistics were achieved by collecting samples using a 0.02º 2θ step scan from 1.5 – 60º with an exposure time of 10 s per step. No peaks could be resolved from the baseline for 2θ > 35º therefore this region was not considered for further analysis.
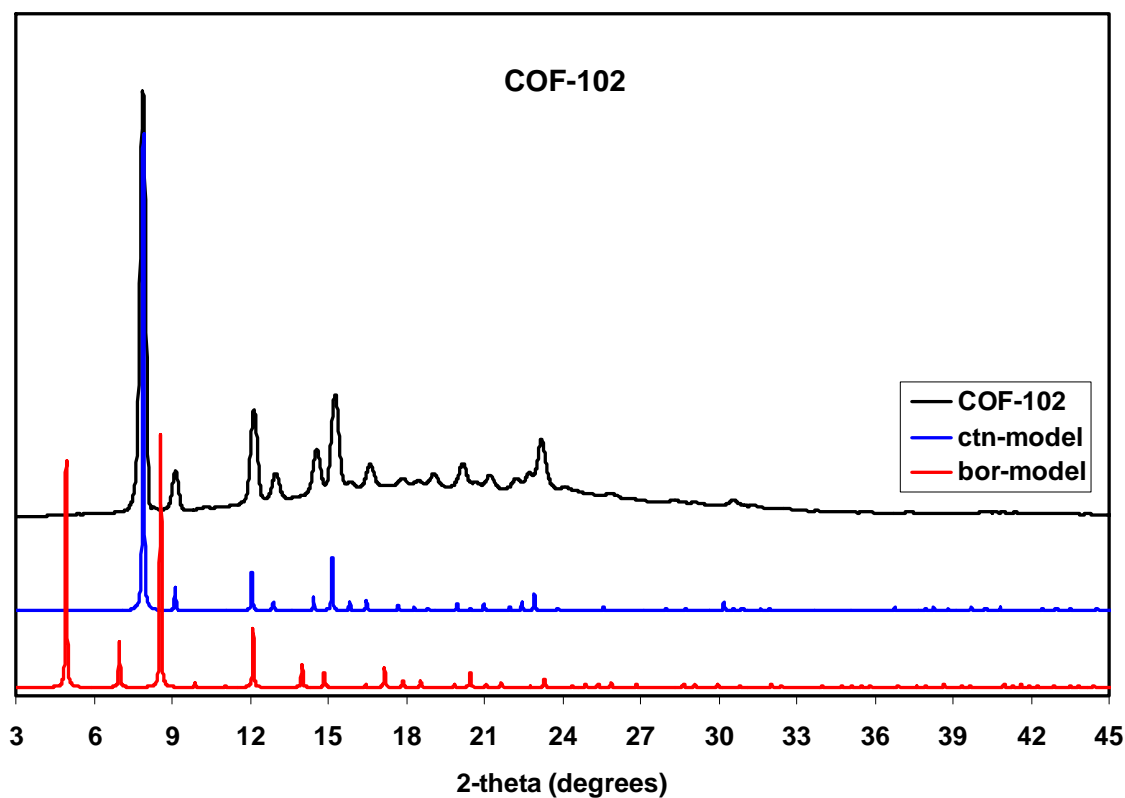
Figure S1: PXRD pattern of COF-102 as synthesized before activation and removal of guests from the pores. Note that the large amorphous background arises from disordered guests in the pores.
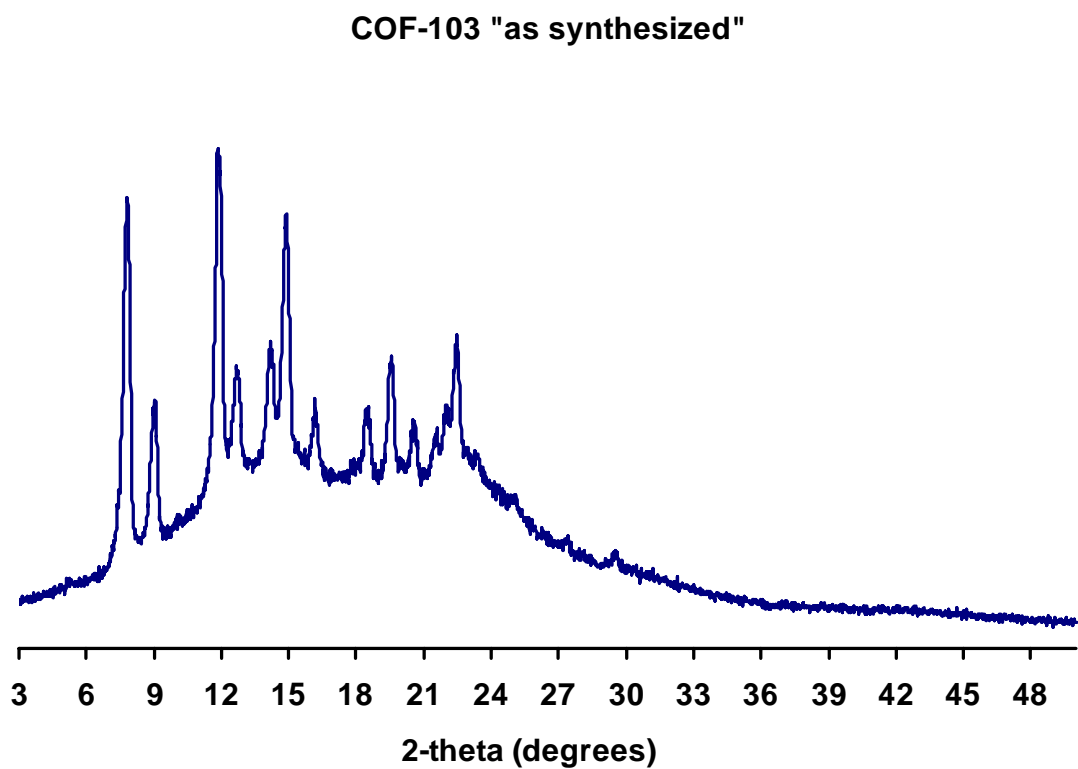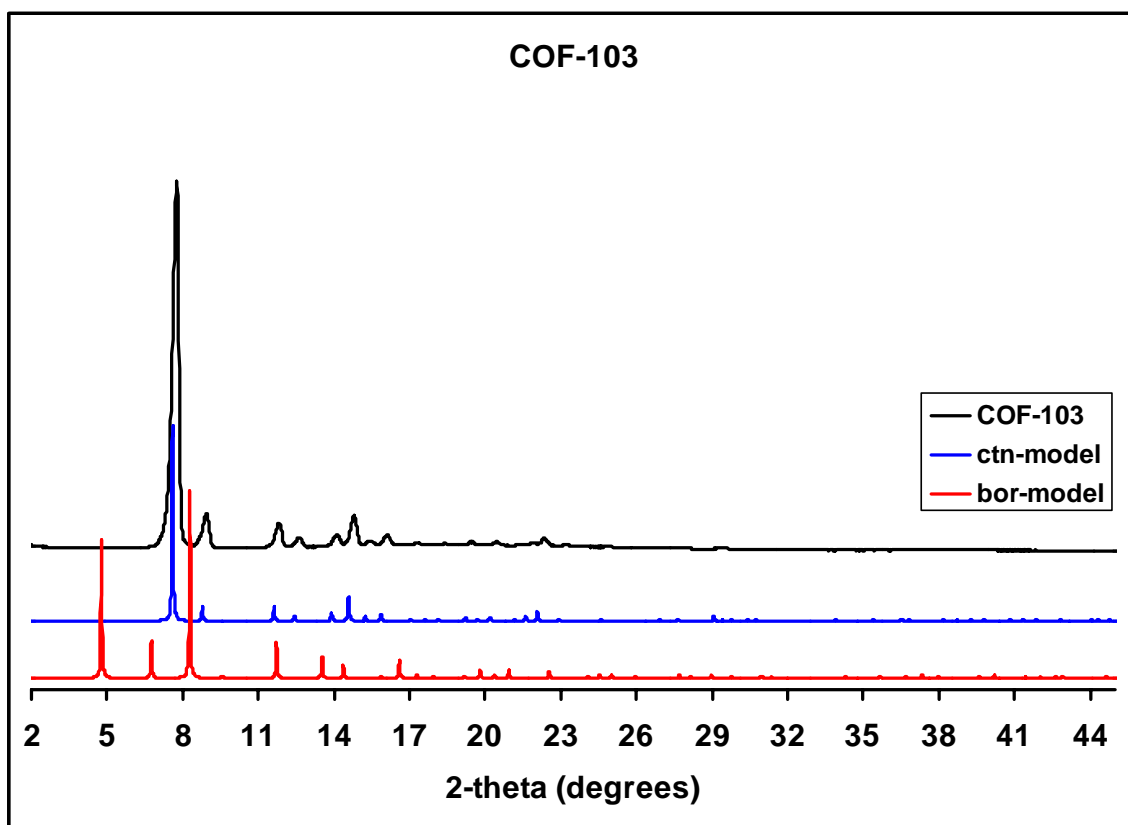

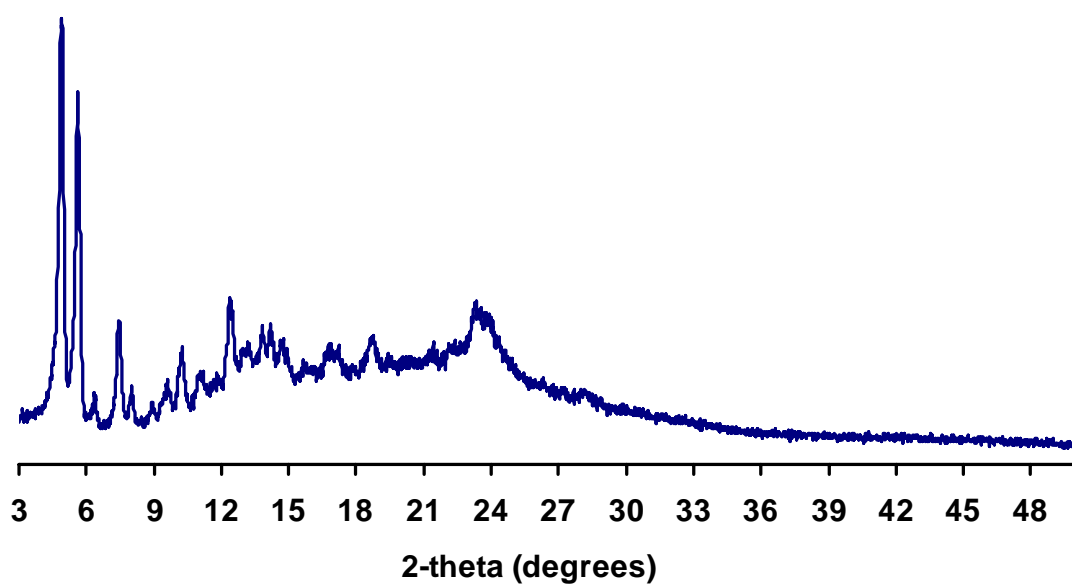
COF-102 "as synthesized"

2-theta (degrees)
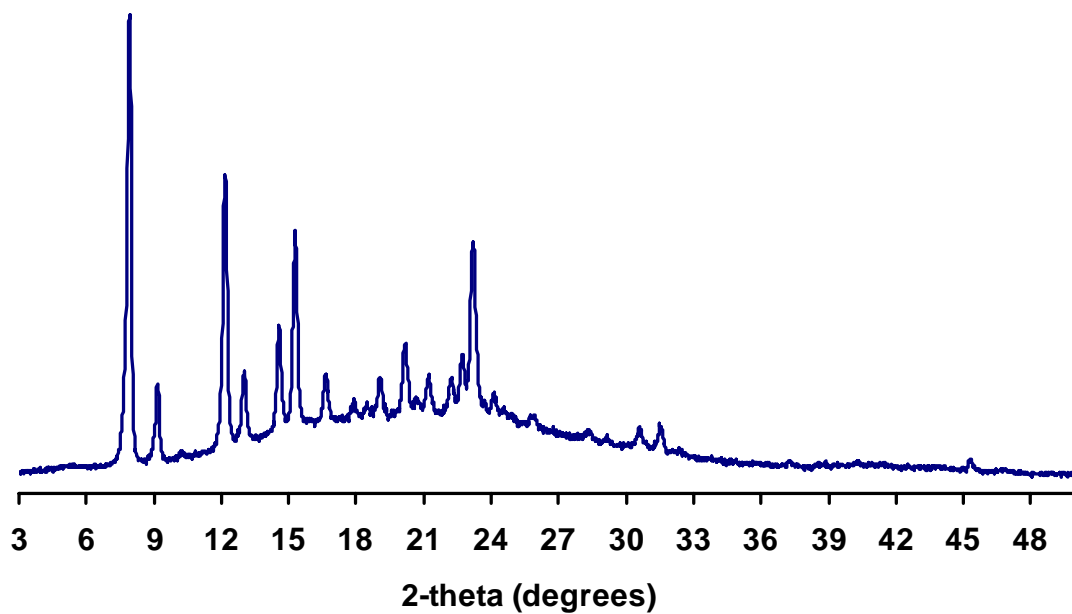
Figure S2: PXRD pattern of evacuated COF-102 (top) compared to patterns calculated from *Cerius*[2] for potential **ctn** and **bor** structures, **ctn** topology (middle), and **bor** topology (bottom). Note the pattern from the **bor** model does not match the pattern of COF-102. Note that the experimental pattern matches that for the **ctn-**model, and emergence of the flat baseline with removal of guests from the pores.
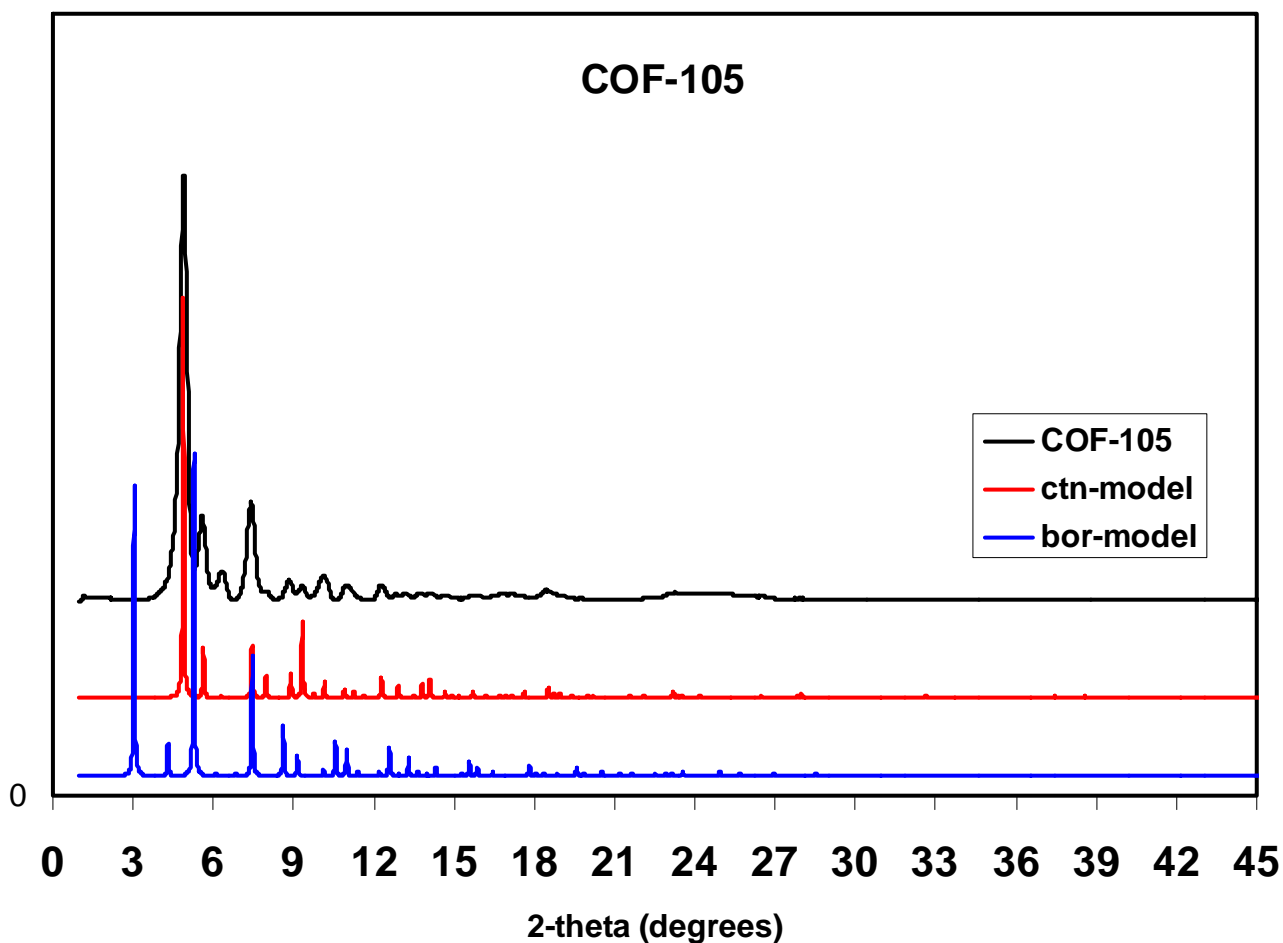
Figure S3: PXRD pattern of COF-103 as synthesized before activation and removal of guests from the pores. Note the large amorphous background arises from disordered guests in the pores.
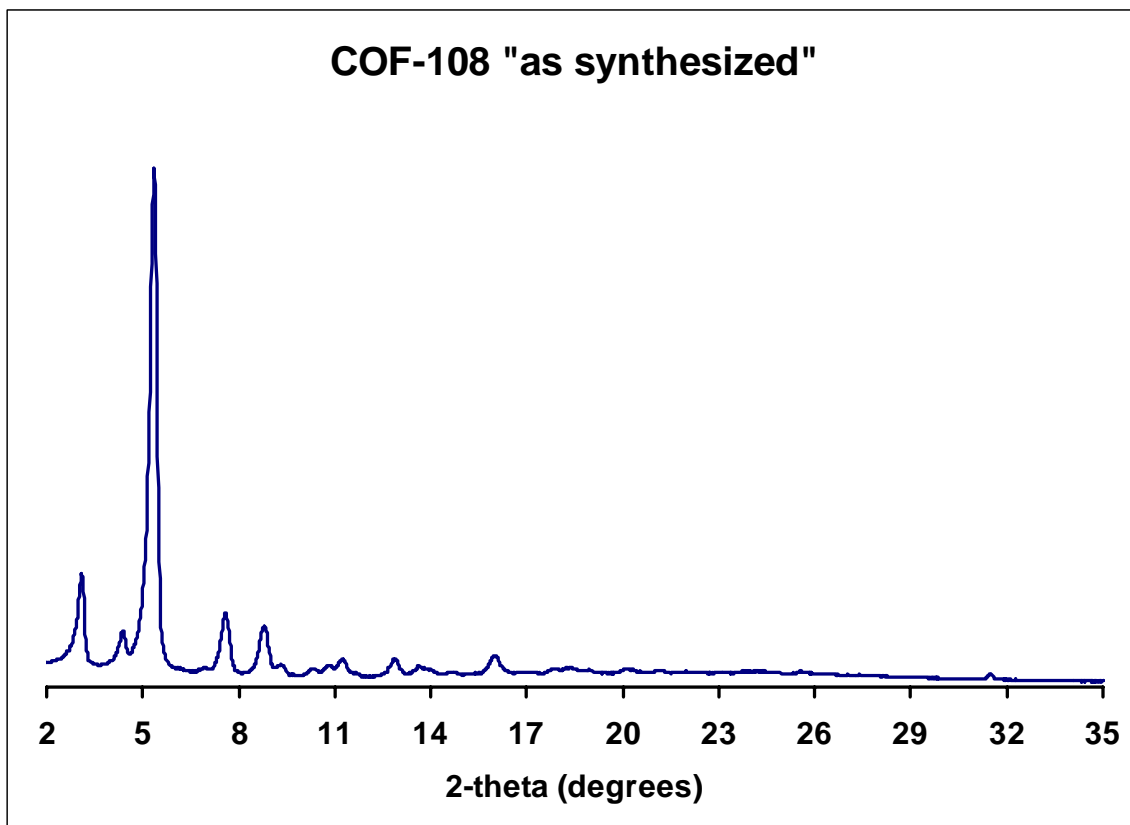
COF-103 "as synthesized"

2-theta (degrees)

Figure S4: PXRD pattern of evacuated COF-103 (top) compared to patterns calculated from *Cerius²* for potential **ctn** and **bor** structures, **ctn** topology (middle), and **bor** topology (bottom). Note the pattern from the **bor** model does not match the pattern of COF-103. Note that the experimental pattern matches that for the **ctn-**model, and the emergence of a flat baseline with removal of guests from the pores.

Figure S5: PXRD pattern of COF-105 as synthesized before activation and removal of guest molecules. Note the large amorphous background arises from disordered guests in the pores.

COF-105 "as synthesized"

2-theta (degrees)

Figure S6: PXRD pattern of evacuated COF-105 (top) compared to patterns calculated from *Cerius*[2] for potential **ctn** and **bor** structures, **ctn** topology (middle), and **bor** topology (bottom). Note the pattern from the **bor** model does not match the pattern of COF-105. Note that the experimental pattern matches that for the **ctn-**model and the emergence of a flat baseline with removal of guests from the pores.

Figure S7: PXRD pattern of COF-108 as synthesized before activation and removal of guest molecules.

Figure S8: PXRD pattern of "as prepared" COF-108 (top) compared to patterns calculated from *Cerius*[2] for potential **ctn** and **bor** structures, **ctn** topology (bottom), and **bor** topology (middle). Note the pattern from the **bor** matches the experimental pattern of COF-108. Note that the experimental pattern does not match that for the **ctn-**model and the emergence of a flat baseline with removal of guests from the pores
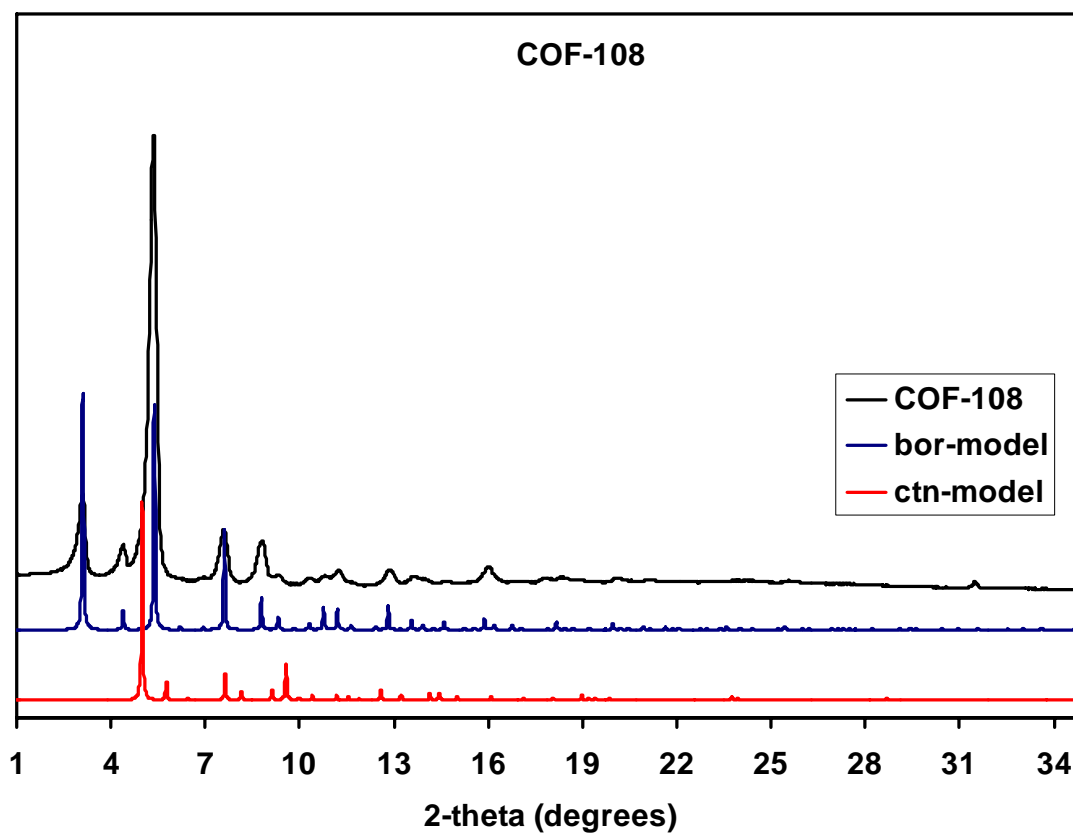
Unit cell determinations were carried out using the Powder-X software suite (PowderX: Windows-95 based program for powder X-ray diffraction data processing) (*5*) for peak selection and interfacing with the Treor (TREOR: A Semi-Exhaustive Trial-and-Error Powder Indexing Program for All Symmetries *ab inito* powder diffraction indexing program (*6*).

Table S5: Calculated and experimental unit cell parameters for COF-102, COF-103, COF-105, and COF-108.

Unit cell Parameter	*Cerius²*	Treor	Le Bail
COF-102, Cubic, $I\bar{4}3d$			
$a = b = $ c (Å)	27.4081	28.00(9)	27.177(1)
COF-103, Cubic, $I\bar{4}3d$			
$a = b = $ c (Å)	28.4550	28.42(4)	28.247(2)
COF-105, Cubic, $I\bar{4}3d$			
$a = b = $ c (Å)	44.3818	45.1(8)	44.886(5)
COF-108, Cubic, $P\bar{4}3m$			
$a = b = $ c (Å)	28.4410	27.7(9)	28.401(5)

Le Bail extractions were conducted using the GSAS program using data up to $2\theta = 35$ degrees. Backgrounds where hand fit with six terms applying a shifted Chebyschev Polynomial. Both profiles where calculated starting with the unit cell parameters indexed from the raw powder patterns and the atomic positions calculated from *Cerius²*. Using the model-biased Le Bail algorithm, F_{obs} were extracted by first

refining peak asymmetry with Gaussian peak profiles, followed by refinement of polarization with peak asymmetry. Unit cells were then refined with peak asymmetry and polarization resulting in convergent refinements. Once this was achieved unit cell parameters were refined followed by zero-shift. Refinement of unit cell parameters, peak asymmetry, polarization and zero-shift were used for the final profiles.

Table S6: Final statistics from Le Bail extractions of COF-102, COF-103, COF-105, and COF-108 PXRD data.

	COF-102	**COF-103**	**COF-105**	**COF-108**
R_p	8.79	7.33	4.64	7.70
wR_p	12.78	16.85	6.91	11.08
χ^2	53.58	43.76	17.13	65.37

Materials and Methods Section S3: *Full synthetic procedures for the preparation of*

COF-102, COF-103, COF-105, and COF-108.

General Synthetic Procedures: All starting materials and solvents, unless otherwise noted, were obtained from the Aldrich Chemical Co. and used with out further purification. Tetrahydrofuran was distilled from sodium benzophenone ketyl, acetone was distilled from anhydrous $Ca(SO_4)$. *Tetra*(4-(dihydroxy)borylphenyl)silane and tetra(4-(dihydroxy)borylphenyl)methane were prepared according to literature method (*7*), COF-5 was prepared according to methods described by A.P. Côté *et al* (*8*). The isolation and handling of all products were performed under an inert atmosphere of nitrogen using either glovebox or Schlenk line techniques. Yields reported here are un-optimized.

Synthesis of COF-102. A Pyrex tube measuring o.d. × i.d. = 10 × 8 mm^2 was charged with *tetra*(4-(dihydroxy)borylphenyl)methane (50.0 mg, 0.10 mmol) and 1.0 mL of a 1:1 v:v solution of mesitylene:dioxane. The tube was flash frozen at 77 K (LN_2 bath), evacuated to an internal pressure of 150 mTorr and flame sealed. Upon sealing the length of the tube was reduced to *ca.* 18 cm. The reaction mixture was heated at 85 °C for 4 days to afford a white precipitate which was isolated by filtration over a medium glass frit and washed with anhydrous tetrahydrofuran (10 mL). The product was immersed in anhydrous tetrahydrofuran (10 mL) for 8 h, during which the activation solvent was decanted and freshly replenished four times. The solvent was removed under vacuum at room temperature to afford **COF-102** as a white powder (27.8 mg, 65%). Anal. Calcd. for ($C_{25}H_{16}B_4O_4$): C, 70.88; H, 3.81. Found: C, 64.89; H, 3.76.

Synthesis of COF-103. In a fashion similar to the preparation of **COF-102**, treatment of

tetra(4-(dihydroxy)borylphenyl)silane (55.0 mg, 0.10) in 1.5 mL of a 3:1 v:v solution of mesitylene:dioxane at 85 °C/150 mTorr for 4 days afforded **COF-103** as a white powder (37.0 mg, 73%) after purification by the described method above. Anal. Calcd. for ($C_{24}H_{16}B_4O_4Si$): C, 65.56; H, 3.67. Found: C, 60.43; H, 3.98.

Synthesis of COF-105. In a fashion similar to the preparation of **COF-102**, treatment of *tetra*(4-(dihydroxy)borylphenyl)silane (26.0 mg, 0.05 mmol) with 2,3,6,7,10,11-hexahydroxytriphenylene [(HHTP) 23.8 mg, 0.07 mmol, TCI] in 1.0 mL of a 1:1 v:v solution of mesitylene:dioxane at 85 °C/150 mTorr for 9 days afforded **COF-105** as a green powder. The product was filtered over a medium glass frit and washed with anhydrous acetone (10 mL) then immersed in anhydrous acetone (20 mL) for 24 h, during which the activation solvent was decanted and freshly replenished two times. The solvent was removed under vacuum at room temperature to afford **COF-105** (26.8 mg, 58% based on the boronic acid). Anal. Calcd. for ($C_{48}H_{24}B_4O_8Si$): C,72.06; H, 3.02. Found: C, 60.39; H, 3.72.

Synthesis of COF-108. In a fashion similar to the preparation of **COF-102**, treatment of *tetra*(4-(dihydroxy)borylphenyl)methane (25.0 mg, 0.05 mmol) with 2,3,6,7,10,11-hexahydroxytriphenylene [(HHTP) 34.0 mg, 0.10 mmol, TCI] in 1.0 mL of a 1:2 v:v solution of mesitylene:dioxane at 85 °C/150 mTorr for 4 days afforded **COF-108** as a green powder. The product was filtered over a medium glass frit and washed with anhydrous acetone (10 mL) then immersed in anhydrous acetone (20 mL) for 24 h, during which the activation solvent was decanted and freshly replenished two times. The solvent was removed under vacuum at room temperature to afford **COF-108** as a green

powder (30.5 mg, 55% based on the boronic acid). Anal. Calcd. for ($C_{147}H_{72}B_{12}O_{24}$): C, 75.07; H, 3.09. Found: C, 62.80; H, 3.11.

The low carbon values calculated for COF-102, -103, -105, and -108 is commonly encountered with organoboron compounds due to the formation of non-combustible boron carbide byproducts. Error in hydrogen elemental analysis data could be attributed to incomplete removal of solvents and starting materials from the pores.

Activation of COF-102 and COF-103 for gas adsorption measurements. Under an atmosphere of nitrogen, samples of COF-102 (65.0 mg) and COF-103 (65.0 mg) were loaded into a cylindrical quartz cells inside a glovebox then were heated to 60 °C under dynamic vacuum (1.0 x10^{-5} Torr) for 12 h. The samples were back-filled with nitrogen to excluded adsorption of moisture prior Ar adsorption measurements.

Materials and Methods Section S4*: FT-IR Spectroscopy of Starting Materials, Model Compounds, and COFs.*

FT-IR data was used to verify that the products were being produced. By observing the loss of certain stretches like hydroxyl groups expected for condensation reactions as well as the appearance of distinctive functional groups produced by the formation of boroxine and triboronate esters, the formation of the expected products can be confirmed. FT-IR spectra of starting materials, model compounds, and COFs were obtained as KBr pellets using Nicolet 400 Impact spectrometer.

Figure S9: FT-IR spectrum of *tetra*(4-(dihydroxy)borylphenyl)methane.
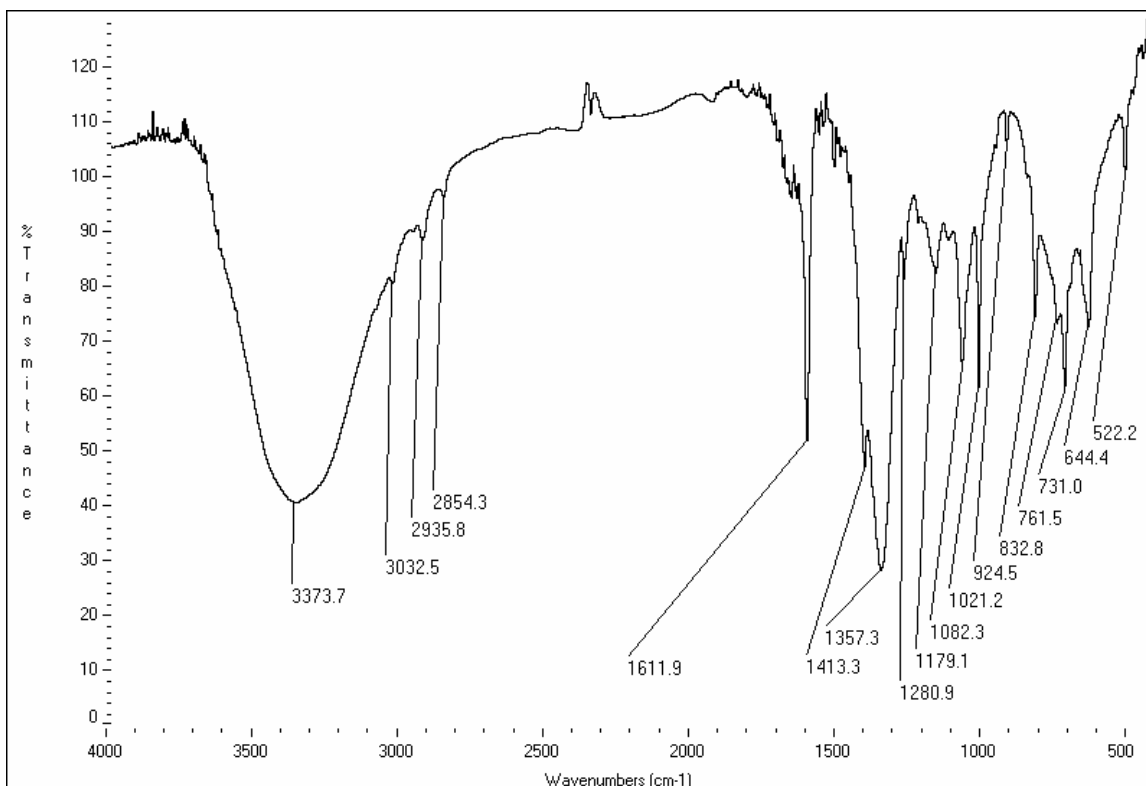
Figure S10: FT-IR spectrum of *tetra*(4-(dihydroxy)borylphenyl)silane
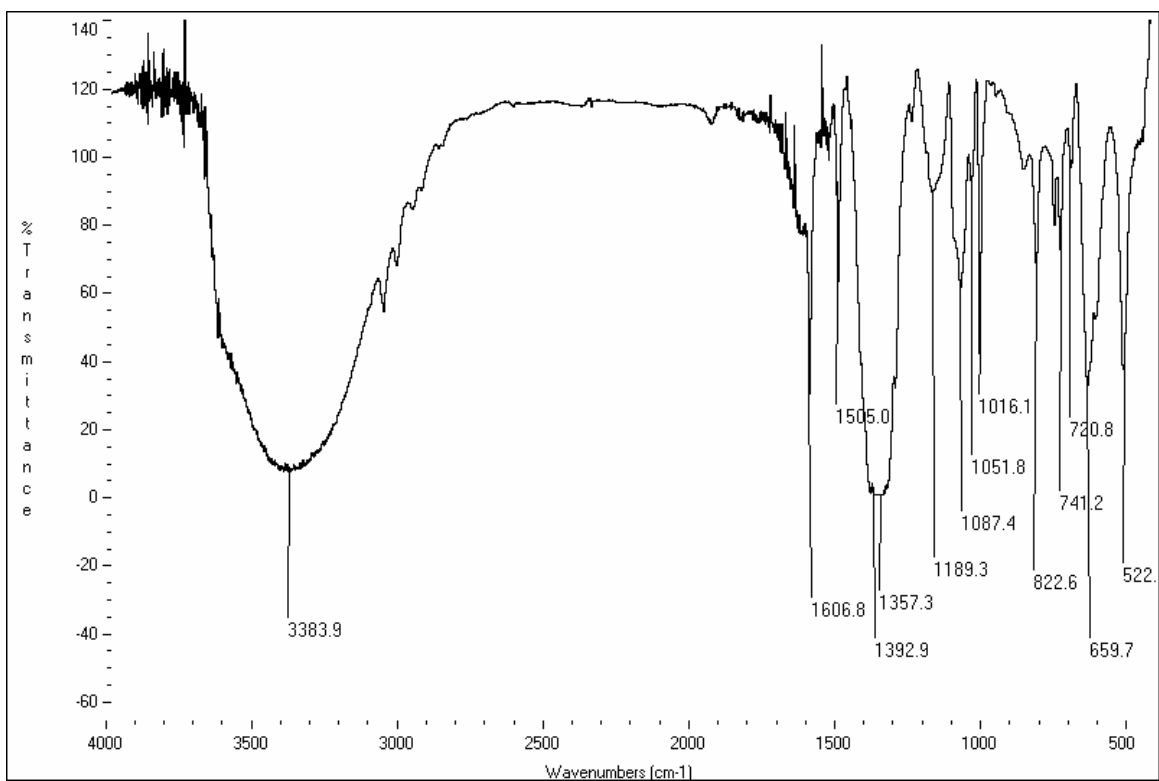
Figure S11: FT-IR spectrum of triphenylboroxine (model compound).
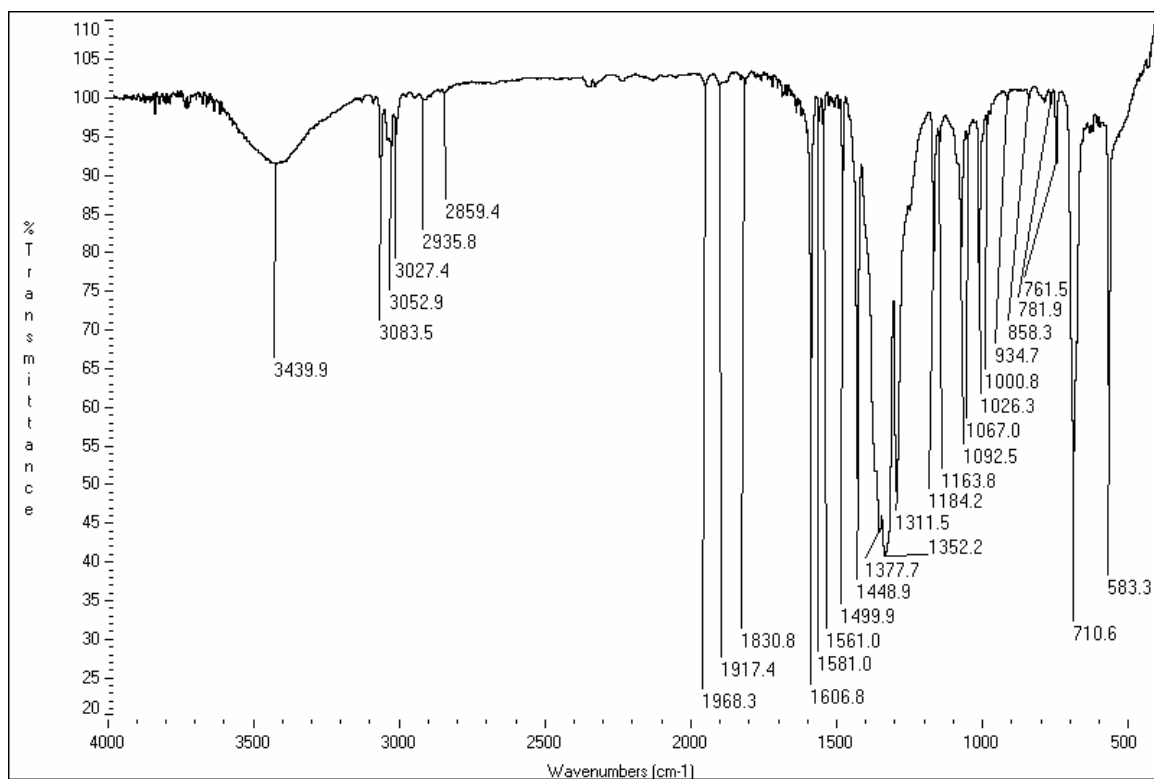
Figure S12: FT-IR spectrum of COF-5 (model compound).
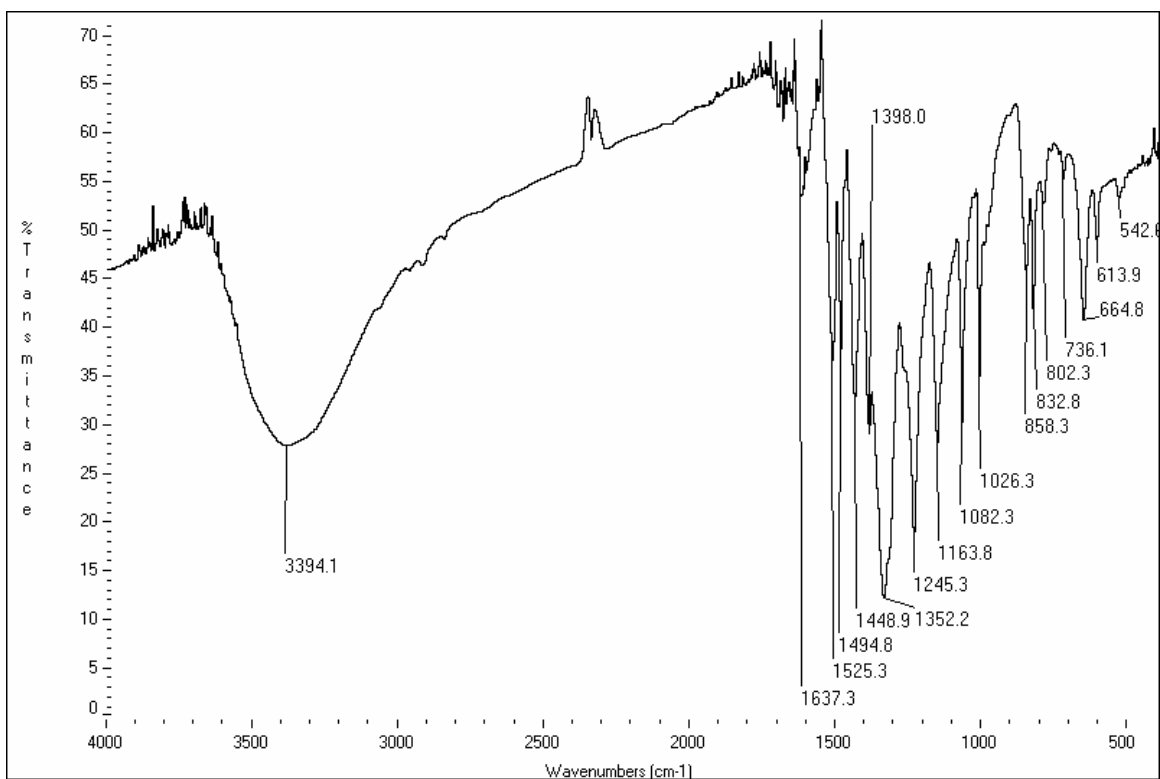
Figure S13: FT-IR spectrum of 2,3,6,7,10,11-hexahydroxytriphenylene (HHTP).
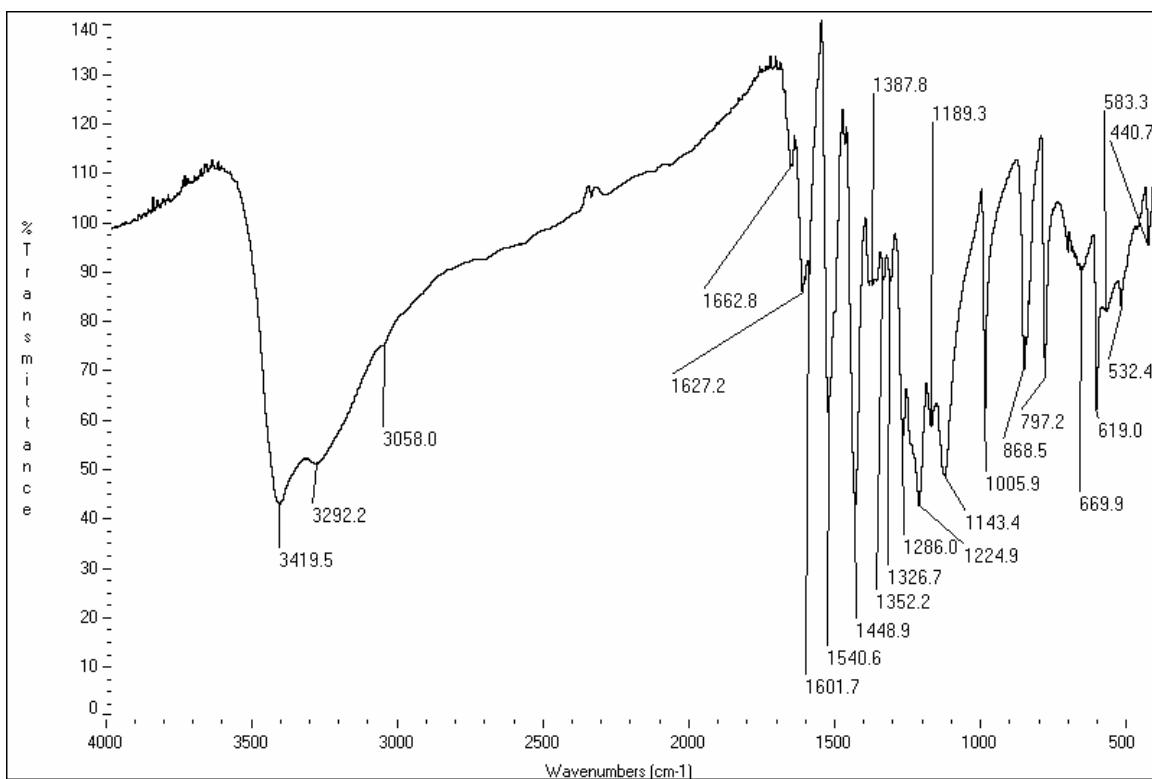
Figure S14: FT-IR spectrum of COF-102. Note that the hydroxyl band stretch of the boronic acid is almost absent indicating a completed consumption of the starting materials. The formation of the B_3O_3 ring is supported by the following IR-bands (cm^{-1}). B-O (1378), B-O (1342), B-C (1226), B_3O_3 (710).
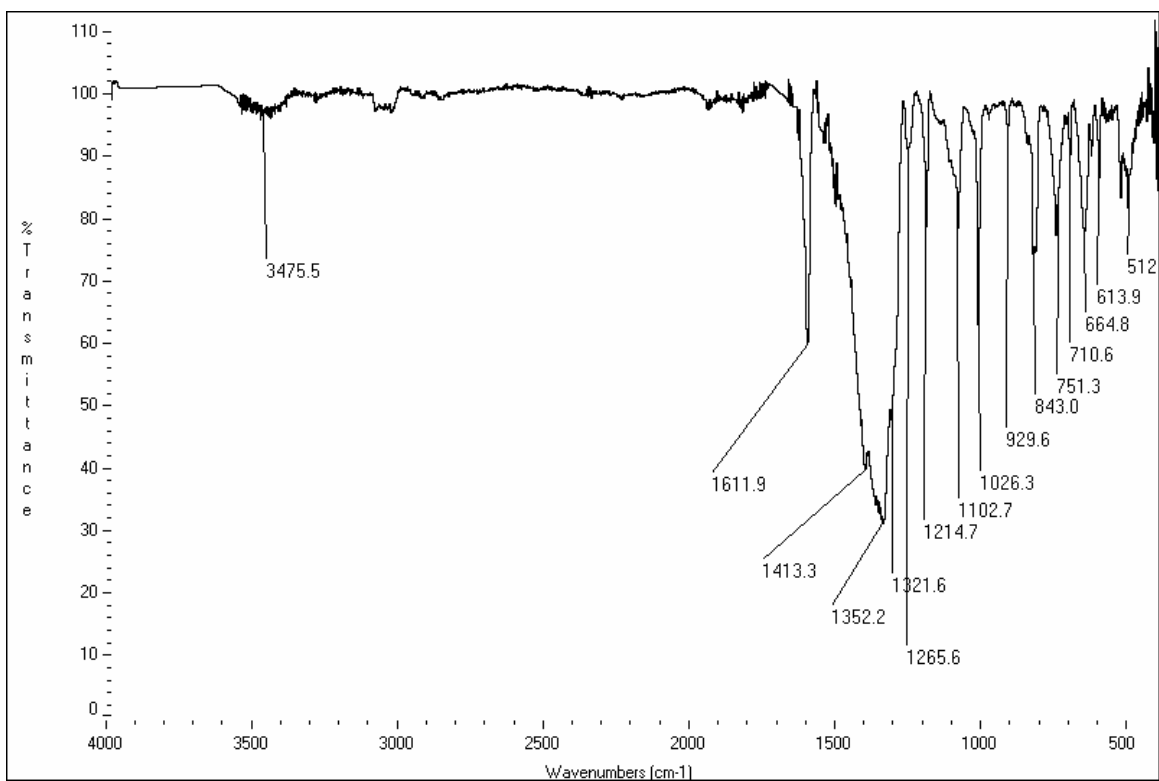
Figure S15: FT-IR spectrum of COF-103. Note that the hydroxyl band stretch of the boronic acid is almost absent indicating a completed consumption of the starting materials. The formation of the B_3O_3 ring is supported by the following IR-bands (cm^{-1}). B-O (1387), B-O (1357), B-C (1226), B_3O_3 (710)
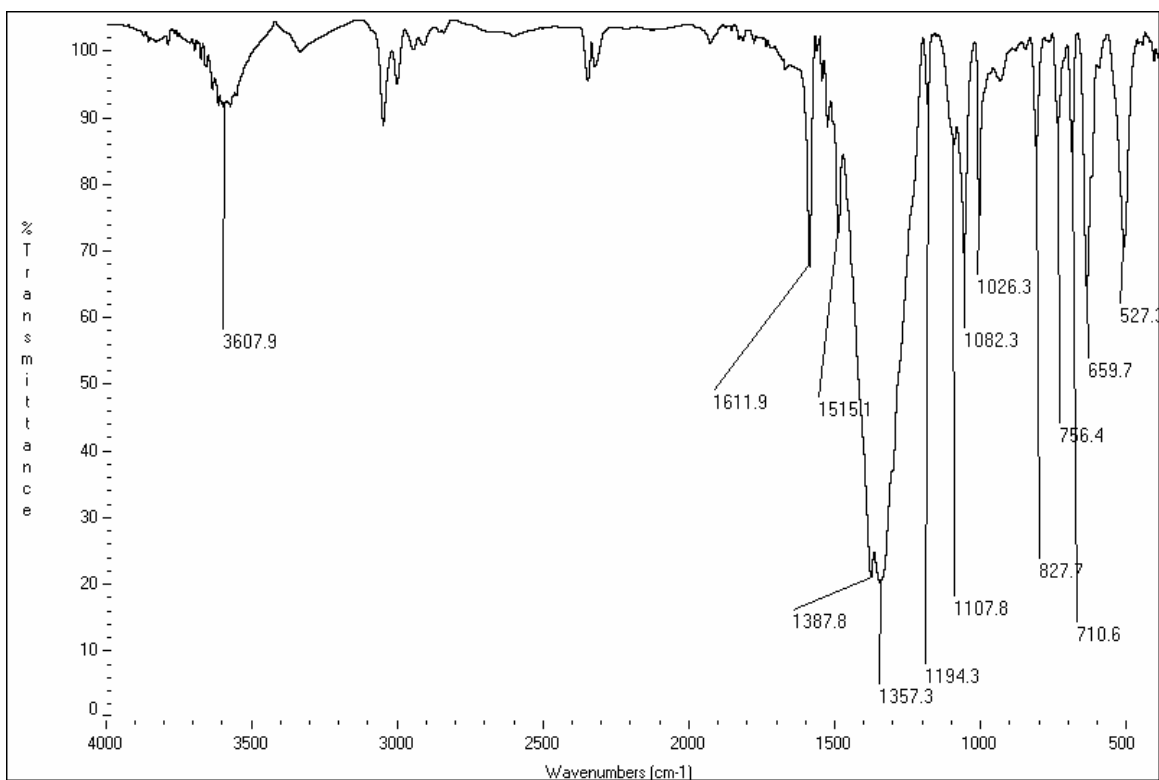
Figure S16: FT-IR spectrum of COF-105. Note that the hydroxyl band stretch of the boronic acid is almost absent indicating a completed consumption of the starting materials. The formation of the C_2B_2O ring is supported by the following IR-bands (cm^{-1}): B-O (1398), B-O (1362), C-O (1245), B-C (1021).
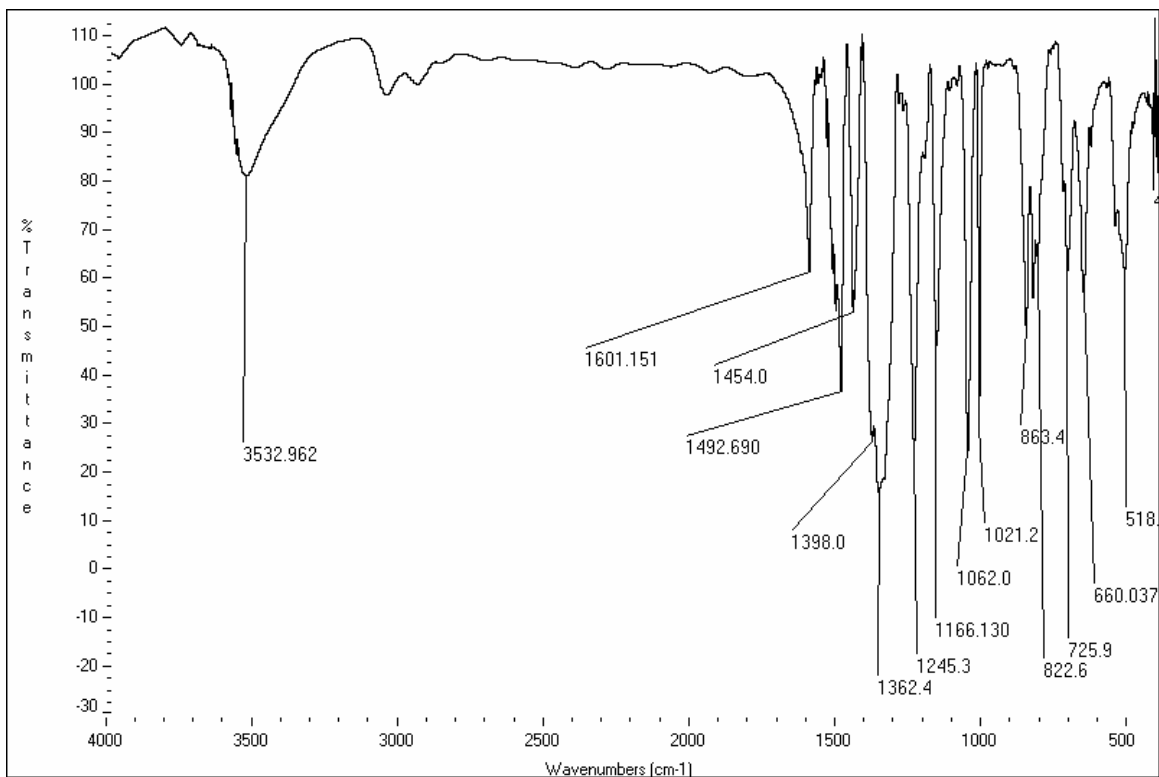
Figure S17: FT-IR spectrum of COF-108. Note that the hydroxyl band stretch of the boronic acid is almost absent indicating a completed consumption of the starting materials. The formation of the C_2B_2O ring is supported by the following IR-bands (cm^{-1}): B-O (1369), C-O (1253), and B-C (1026).
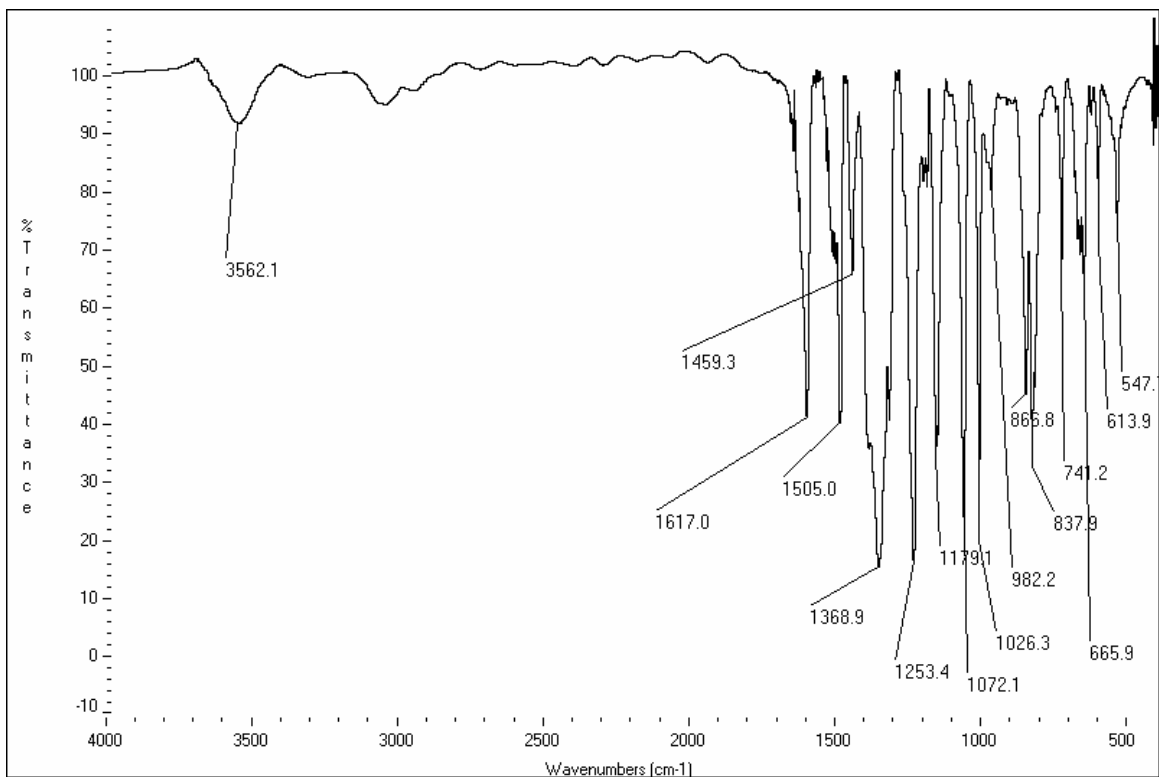
Materials and Methods Section S5: *Solid-State [11]B MQ/MAS, ^{13}C CP/MAS, and [29]Si Nuclear Magnetic Resonance Studies for COF-102, COF-103, COF-105, and COF-108.*

High resolution solid-state nuclear magnetic resonance (NMR) spectra were recorded at ambient temperature on a Bruker DSX-300 spectrometer using a standard Bruker magic angle spinning (MAS) probe with 4 mm (outside diameter) zirconia rotors. Cross-polarization with MAS (CP/MAS) was used to acquire ^{13}C data at 75.47 MHz (*9*). The ^{1}H and ^{13}C ninety-degree pulse widths were both 4 μs. The CP contact time was 1.5 ms. High power two-pulse phase modulation (TPPM) ^{1}H decoupling was applied during data acquisition (*10*). The decoupling frequency corresponded to 72 kHz. The MAS sample spinning rate was 10 kHz. Recycle delays betweens scans varied between 10 and 30 s, depending upon the compound as determined by observing no apparent loss in the ^{13}C signal intensity from one scan to the next. The ^{13}C chemical shifts are given relative to tetramethylsilane as zero ppm, calibrated using the methine carbon signal of adamantane assigned to 29.46 ppm as a secondary reference.

CP/MAS was also used to acquire [29]Si data at 59.63 MHz. [1]H and [29]Si ninety-degree pulse widths of 4.2 μs were used with a CP contact time 7.5 ms. TPPM ^{1}H decoupling was applied during data acquisition. The decoupling frequency corresponded to 72 kHz. The MAS spinning rate was 5 kHz. Recycle delays determined from the ^{13}C CP/MAS experiments were used for the various samples. The [29]Si chemical shifts are referenced to tetramethylsilane as zero ppm, calibrated using the trimethylsilyl silicon in tetrakis(trimethylsilyl)silane assigned to -9.8 ppm as a secondary reference.

Multiple quantum MAS (MQ/MAS) spectroscopy was used to acquire [11]B data at 96.29 MHz (*11*, *12*). The [11]B solution-state ninety-degree pulse width was 2 μs. TPPM ^{1}H decoupling was applied during data acquisition. The decoupling frequency

corresponded to 72 kHz. The MAS spinning rate was 14.9 kHz. A recycle delay of 3 s was used. The ^{11}B chemical shifts are given relative to BF$_3$ etherate as zero ppm, calibrated using aqueous boric acid at pH = 4.4 assigned to -19.6 ppm as a secondary reference.
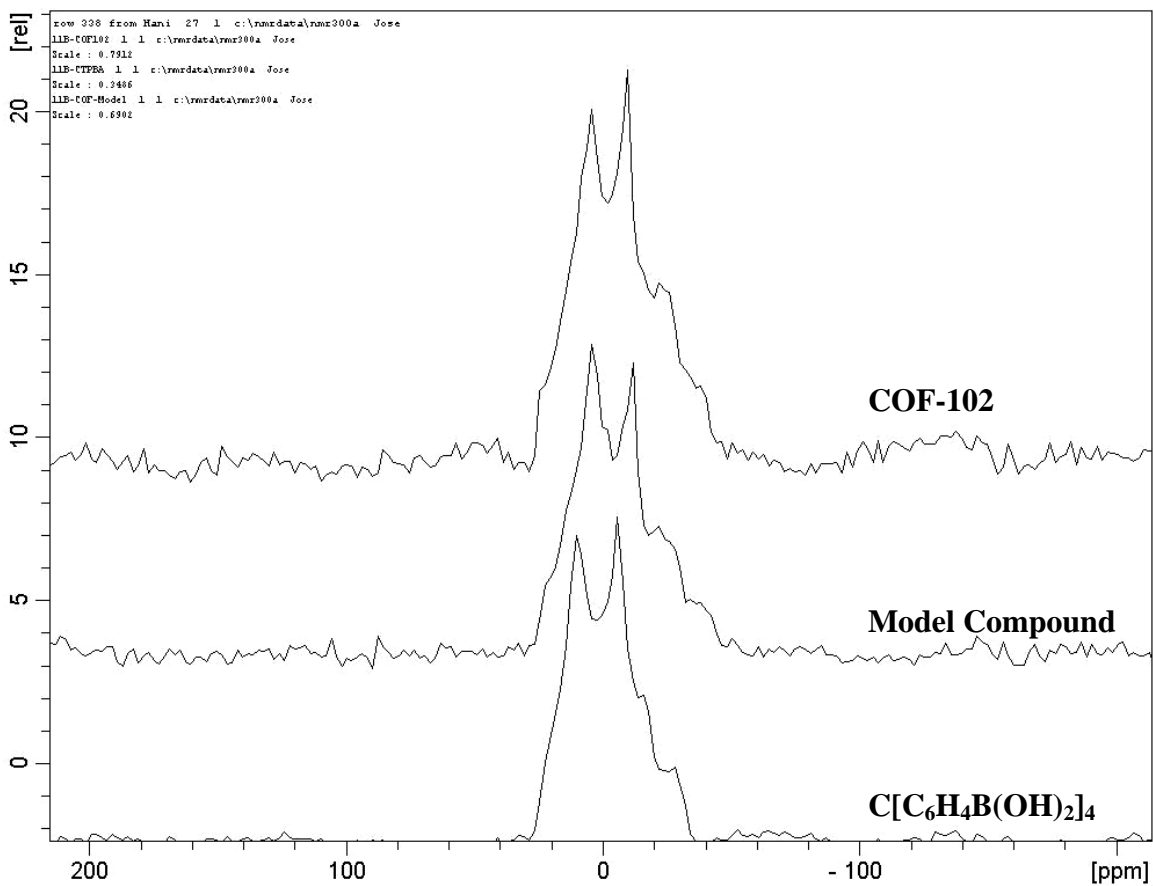
Figure S18: Solid-state ^{11}B NMR spectrum for tetra(4-(dihydroxy)borylphenyl)methane.
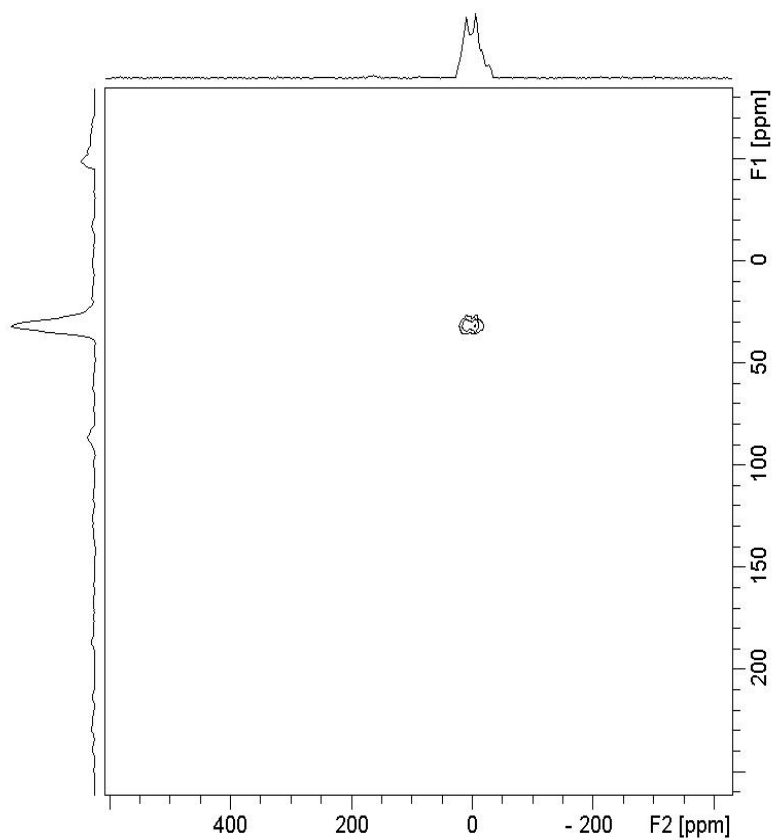
The presence of one signal indicates that only one type of boron species is present in the sample confirming the purity of the starting material.

Figure S19: Solid-state ^{11}B NMR spectrum for triphenylboroxine (model compound).
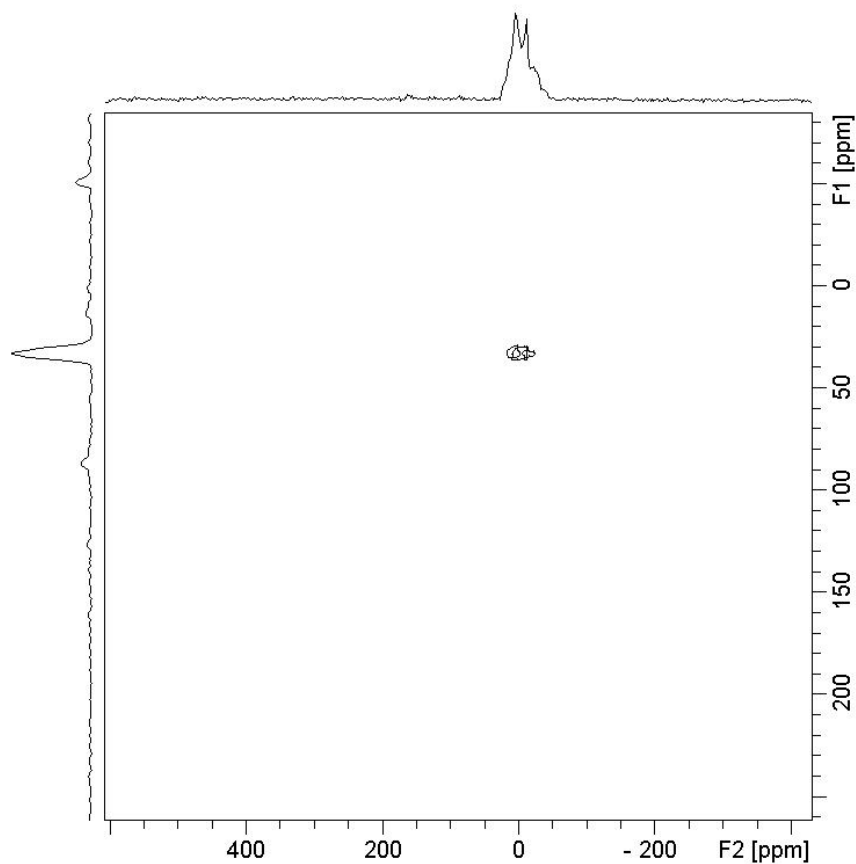
The presence of only one signal indicates that only one type of boron species is present. The peak is slightly shifted in position indicating a change in the environment around the boron, but the similar peak shapes and chemical shift of the boronic acid starting material and the triphenylboroxine indicates that the boron oxygen bonds are still present.

Figure S20: Solid-state ^{11}B NMR spectrum for COF-102.
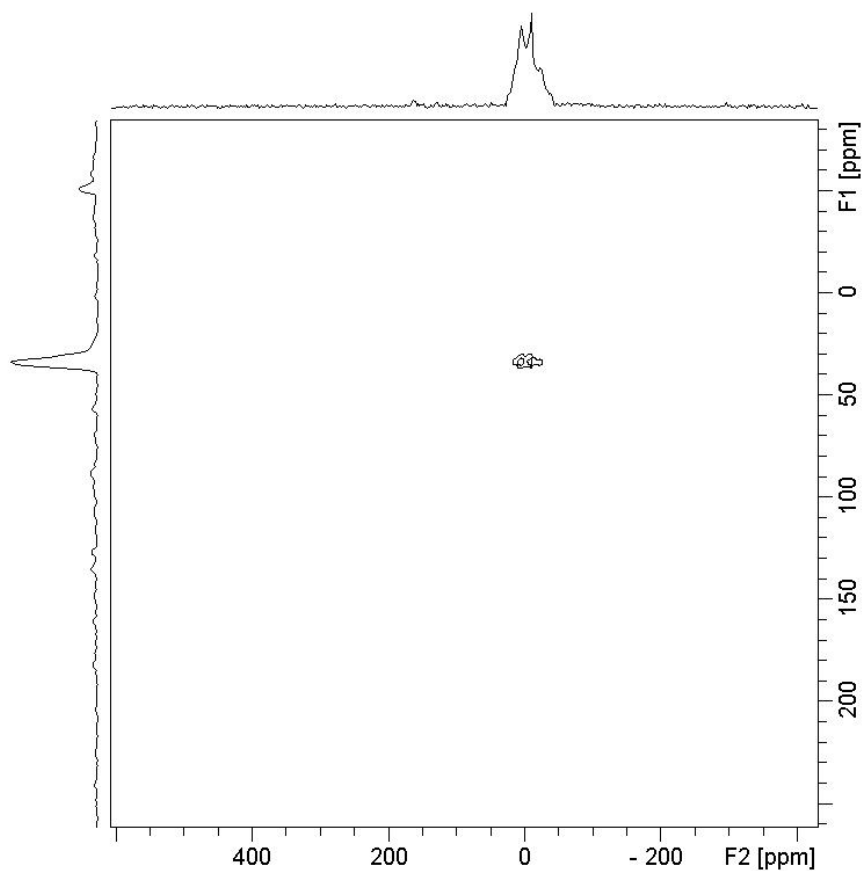
The chemical shift position and peak shape of the single signal match the spectra obtained for the model compound, triphenylboroxine. The single signal indicates that only one type of boron species is present confirming the purity of the product.

Figure S21: Stack plot comparing the ^{11}B NMR spectra of COF-102, triphenylboroxine, and tetra(4-(dihydroxy)borylphenyl)methane.
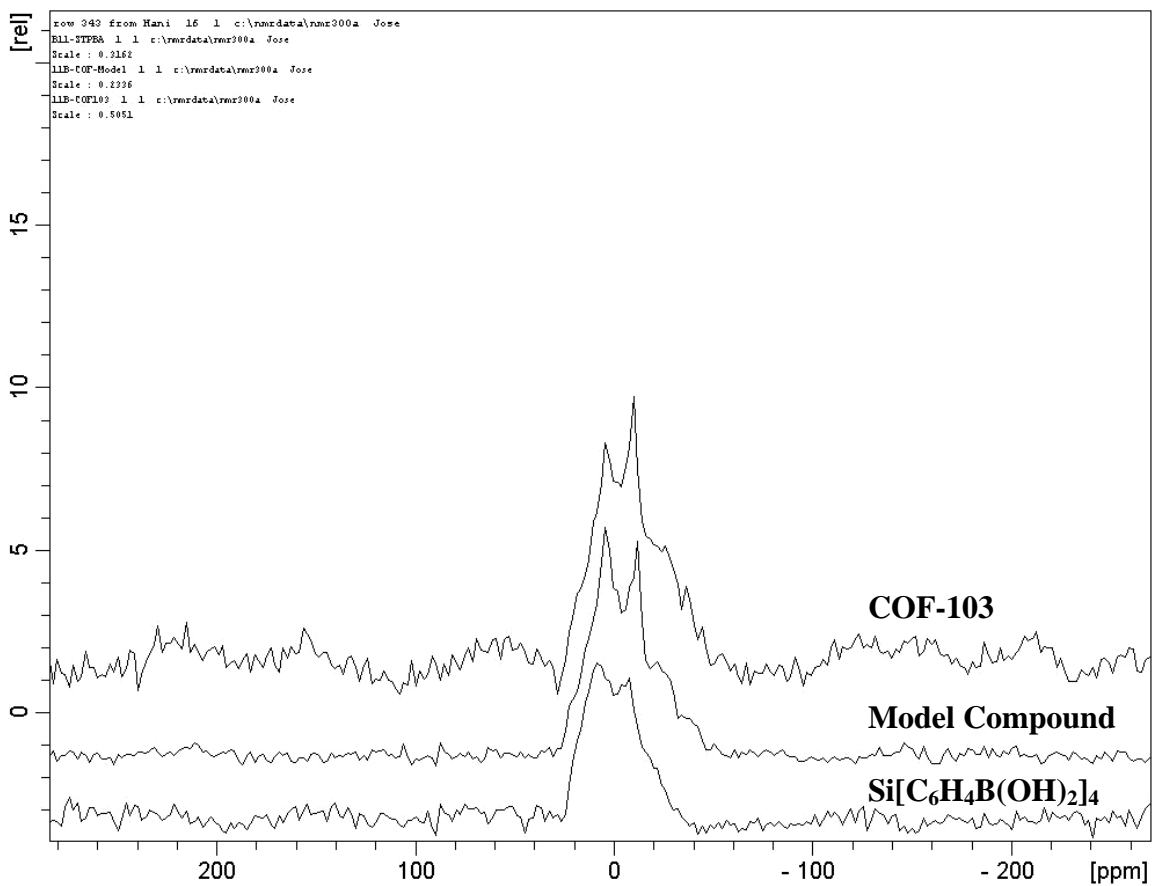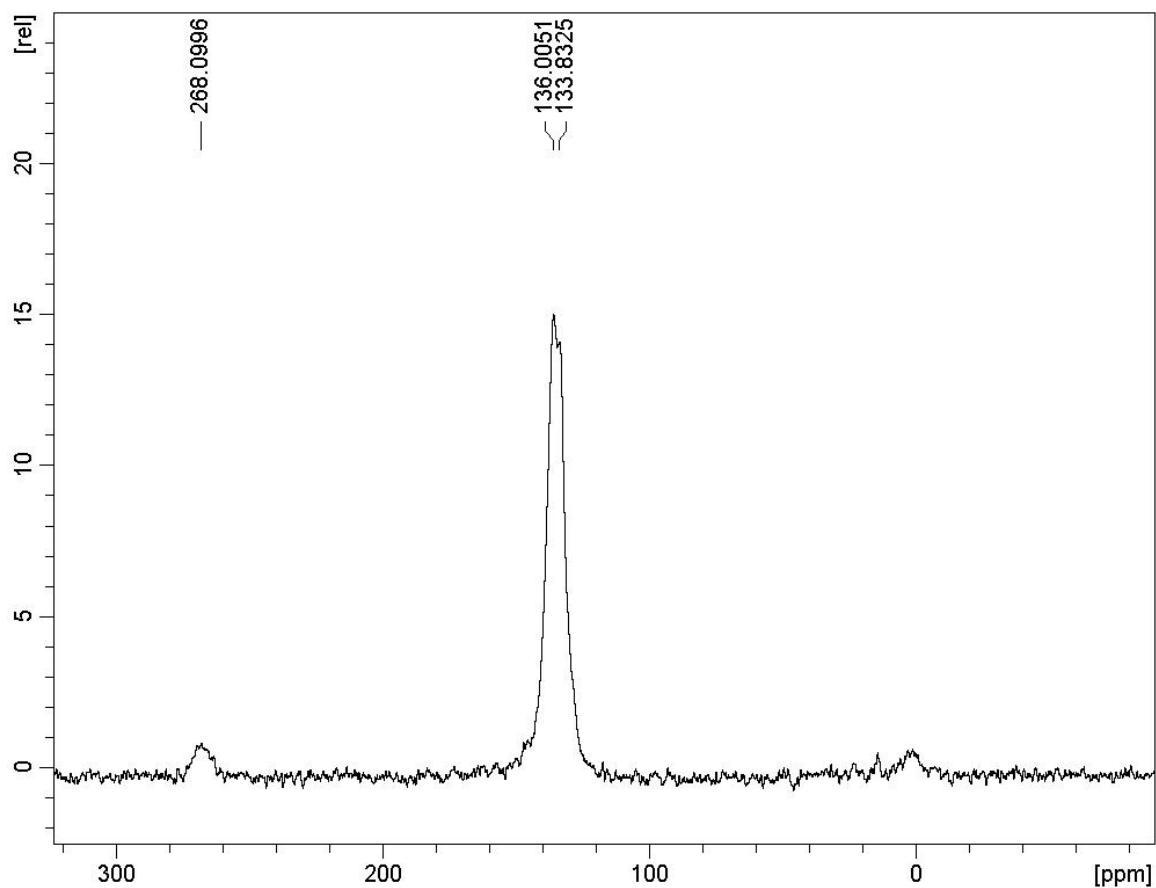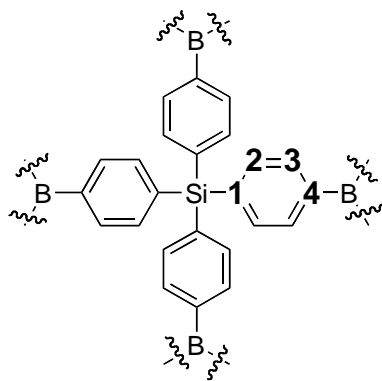
**Figure S22:** Solid-state ^{13}C NMR spectrum for tetra(4-(dihydroxy)borylphenyl)methane.
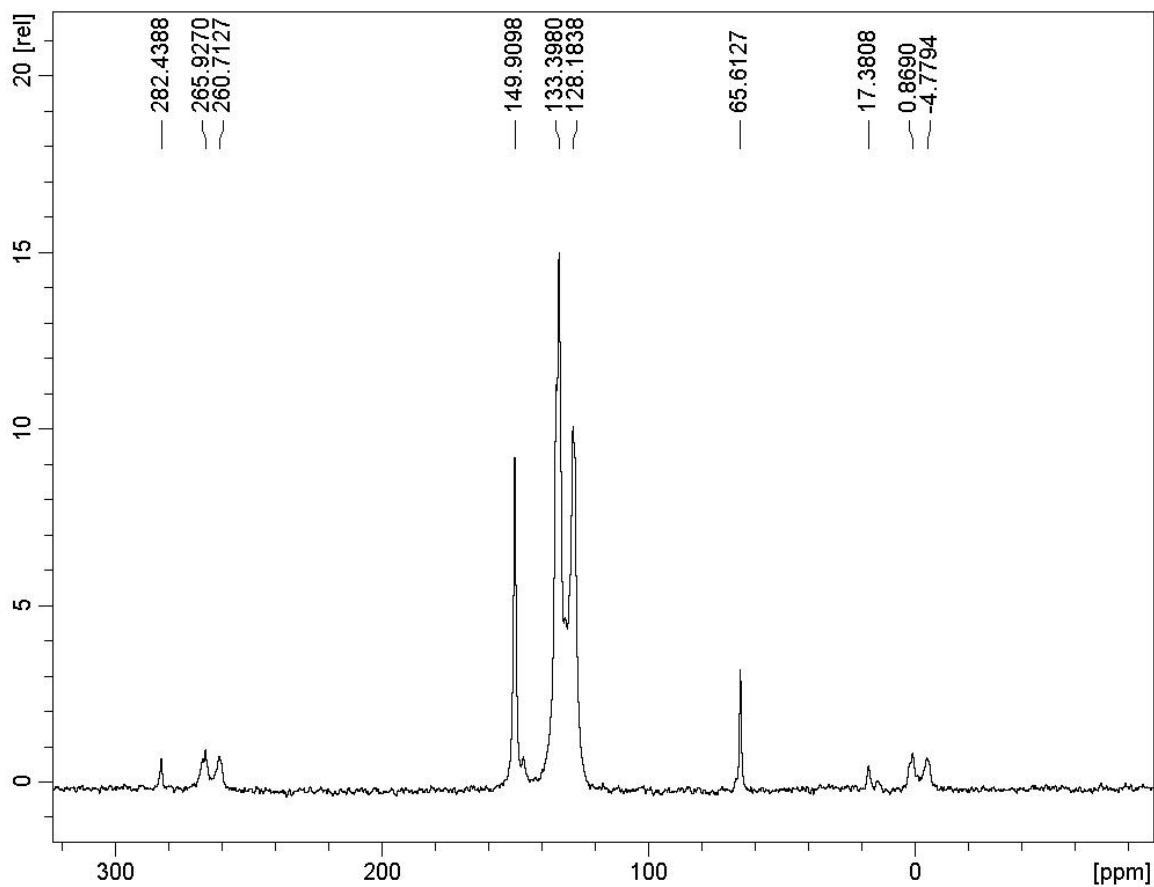
All the expected signals are present and match the predicted chemical shift values.

Spinning side bands are present as well.
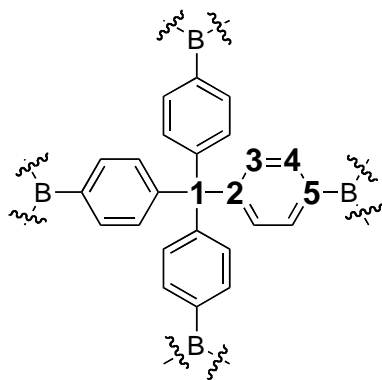
Carbon	Chemical Shift
1	65.61
2	149.90
3	128.18
4	133.40
5	128.18

Figure S23: Solid-state ^{13}C NMR spectrum for COF-102.
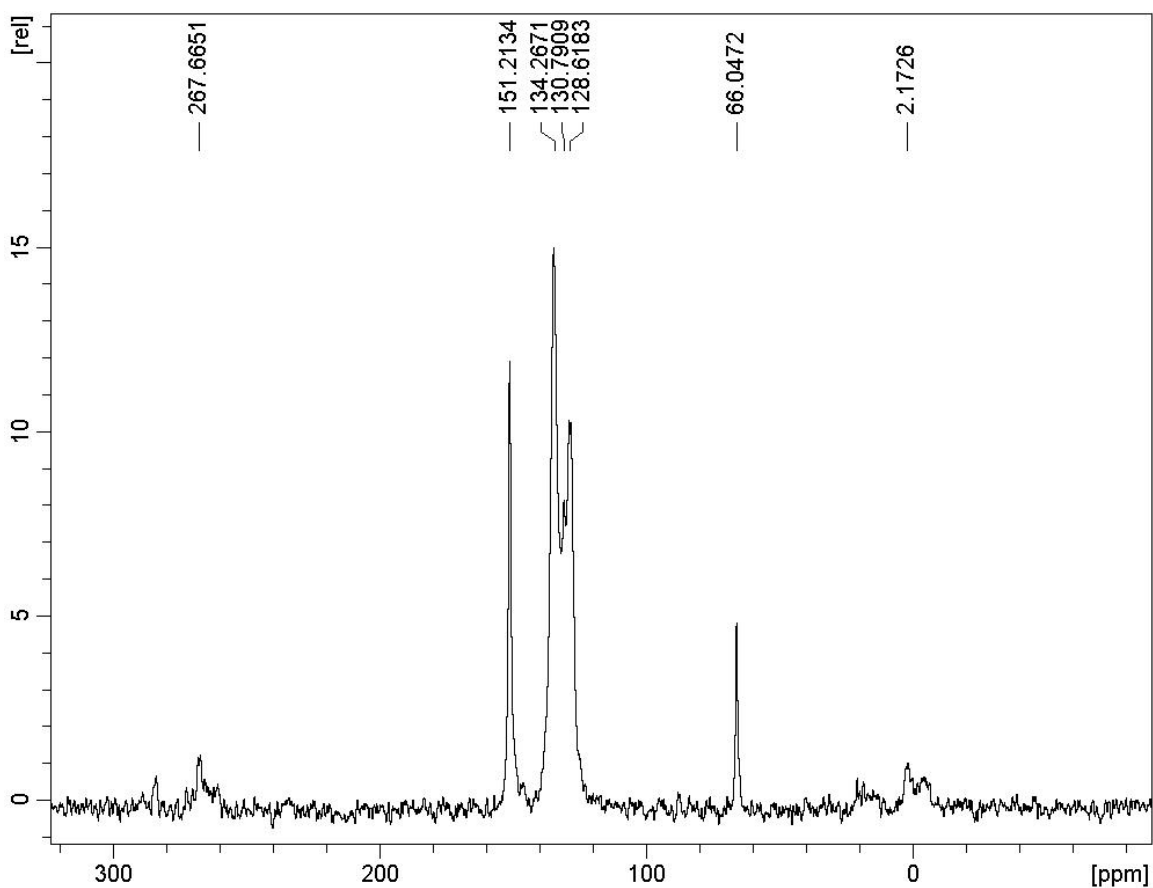
All the signals from the starting boronic acid are present and no other signals are found except spinning side bands indicating the survival of the backbone and purity of the material.
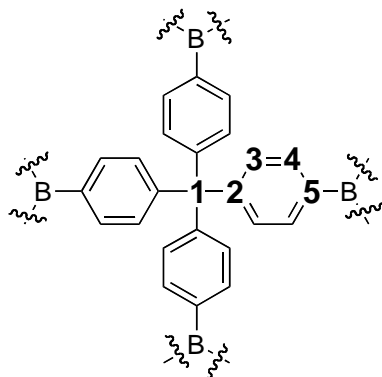
Carbon	Chemical Shift
1	66.0472
2	151.21
3	128.62
4	134.27
5	130.79

Figure S24: Solid-state ^{11}B NMR spectrum for *tetra*(4-(dihydroxy)borylphenyl)silane.
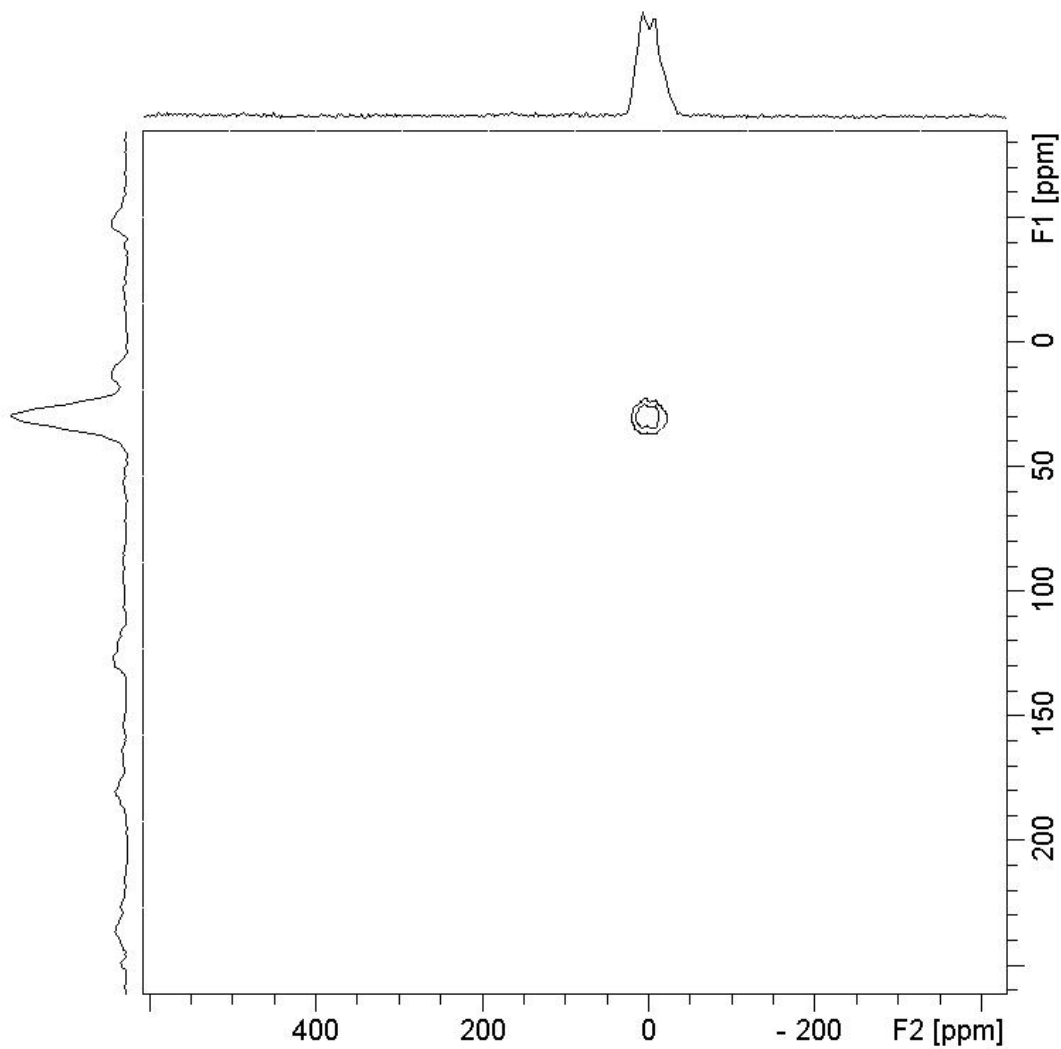
The presence of one signal indicates that only one type of boron species is present in the sample confirming the purity of the starting material.

Figure S25: Solid-state ^{11}B NMR spectrum for COF-103.
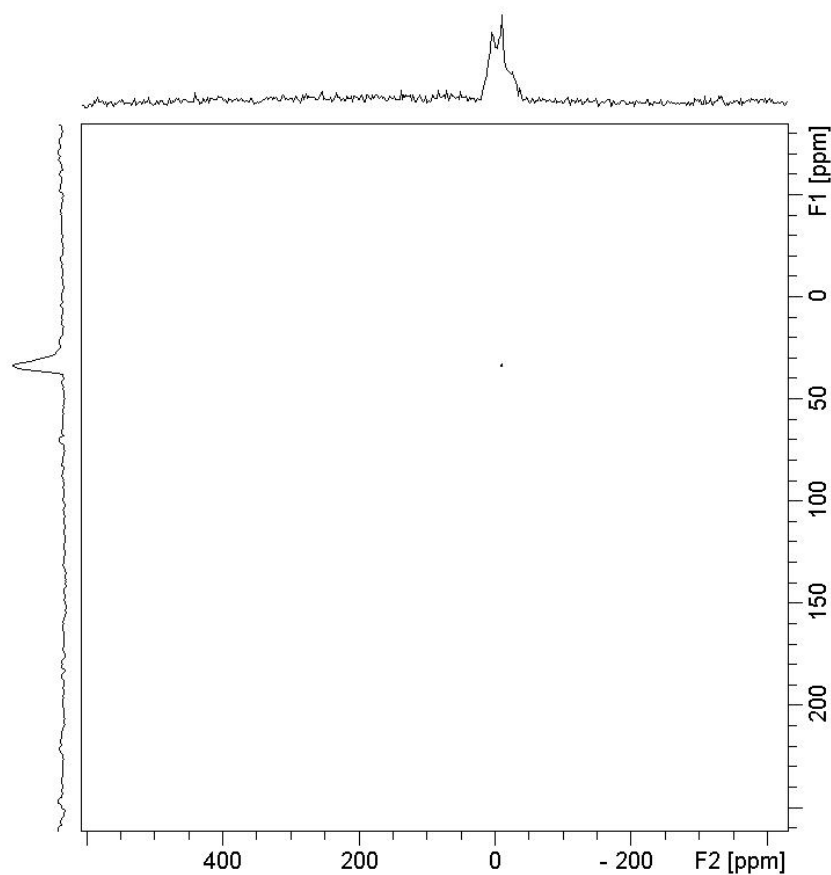
The chemical shift position and peak shape of the single signal match the spectra

obtained for the model compound, triphenylboroxine. The single signal indicates that

only one type of boron species is present confirming the purity of the product.

Figure S26: Stack plot comparing the ^{11}B NMR spectra of COF-103, triphenylboroxine, and *tetra*(4-(dihydroxy)borylphenyl)silane.

Figure S27: Solid-state ^{13}C NMR spectrum for *tetra*(4-(dihydroxy)borylphenyl)silane.

All the expected signals are present and match the predicted chemical shift values.

Spinning side bands are present as well. The separate carbon signals are too close in

chemical shift to be resolved.

Carbon	Chemical Shift
1	136.05
2	133.8
3	133.8
4	133.8

Figure S28: Solid-state ^{13}C NMR spectrum for COF-103.
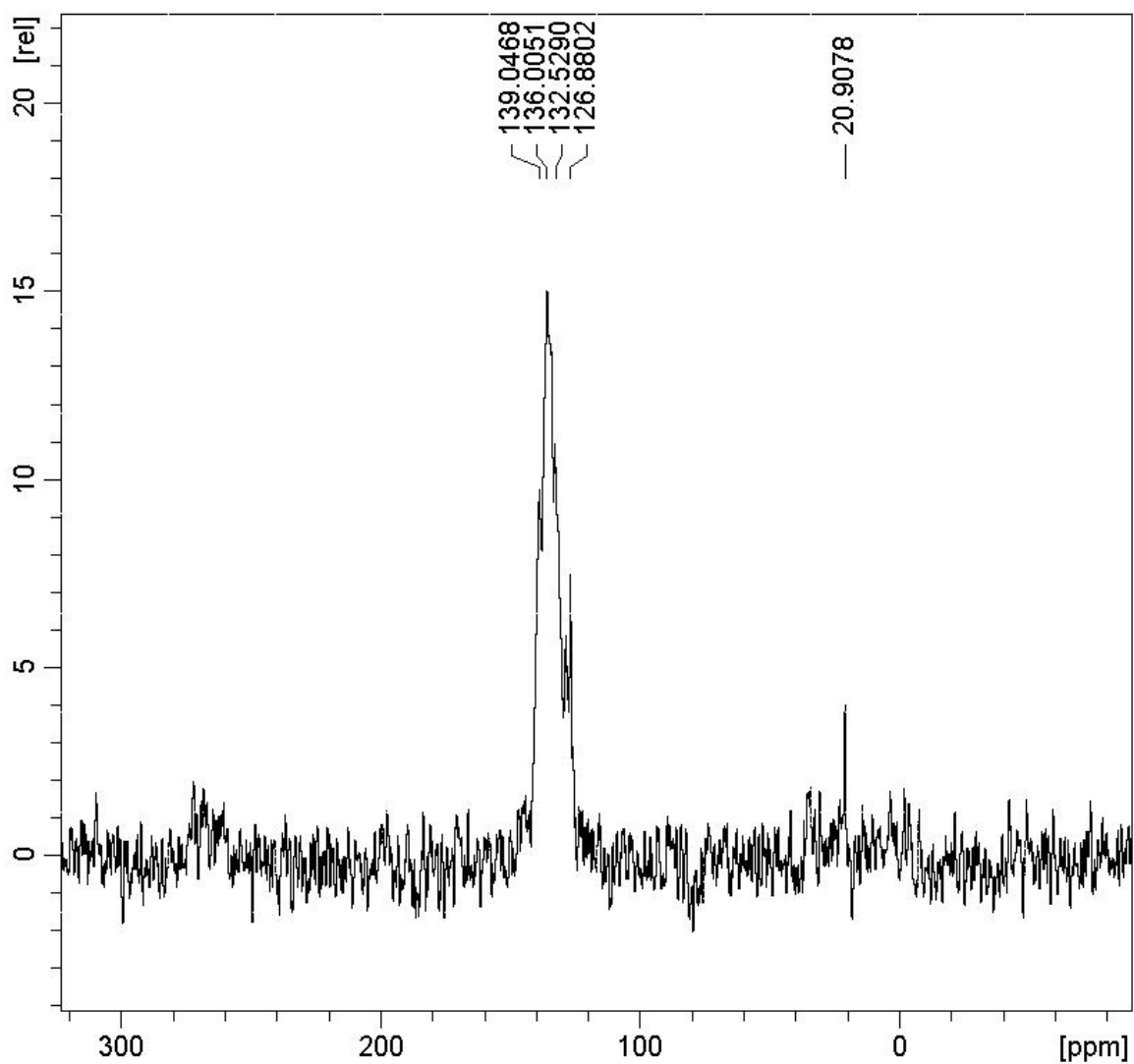
All the signals from the starting boronic acid are present and no other signals are found except spinning side bands indicating the survival of the backbone and purity of the material. The peak at 20 ppm comes from mesitylene inside the structure.
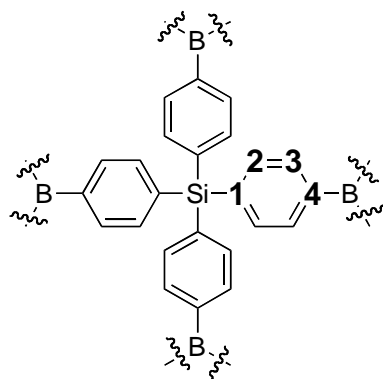
Carbon	Chemical Shift
1	139.05
2	126.88
3	136.00
4	132.53

Figure S29: Solid-state ^{29}Si spectra for COF-103 (top) and tetra(4-(dihydroxy)borylphenyl)silane (bottom). Note that spectrum of COF-103 contains only one resonance for the silicon nuclei exhibiting a chemical shift very similar to that of the tetra(4-(dihydroxy)borylphenyl)silane indicating the integrity of the tetrahedral block and the exclusion of any Si-containing impurities.
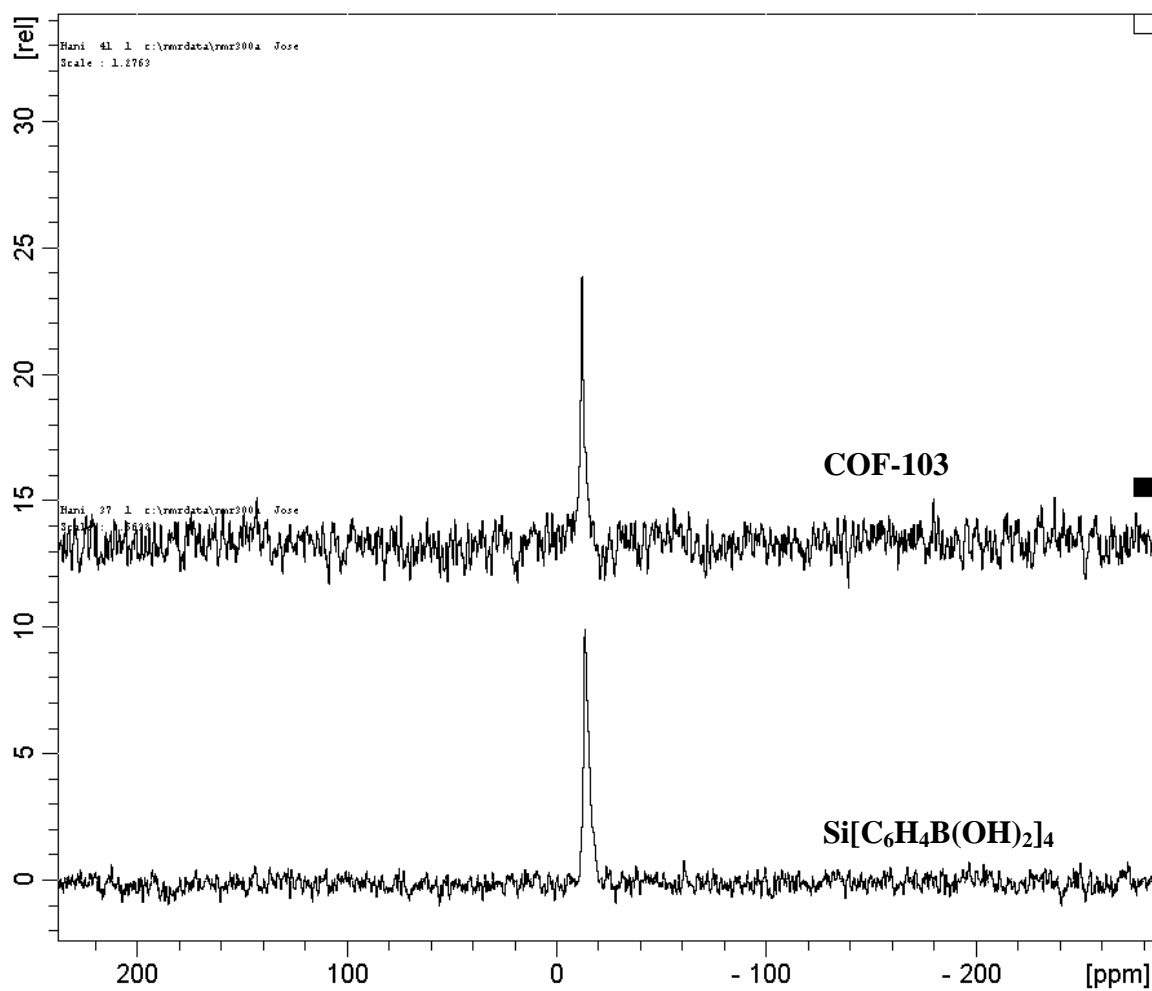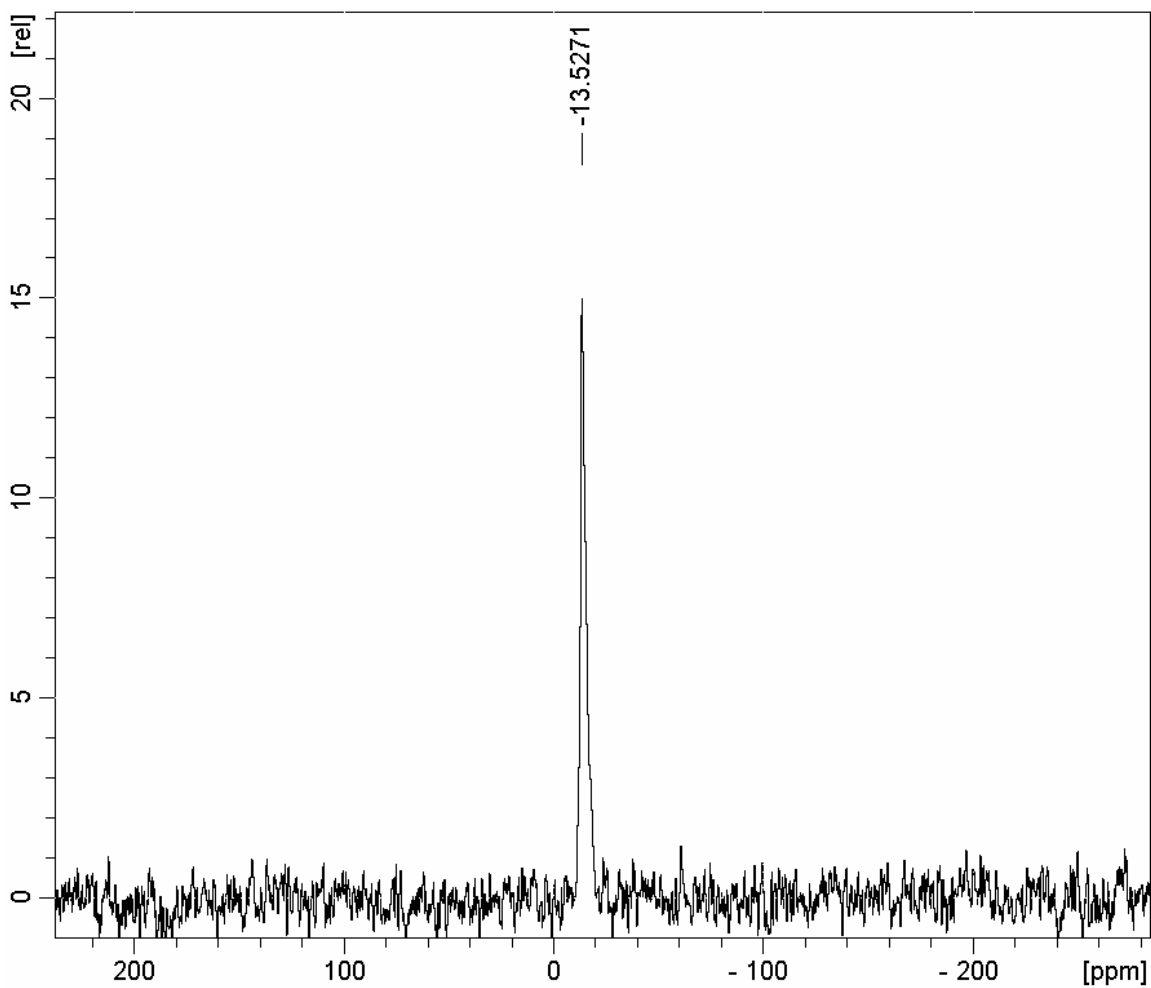
Figure S30: Solid-state ^{29}Si NMR spectrum for COF-103.
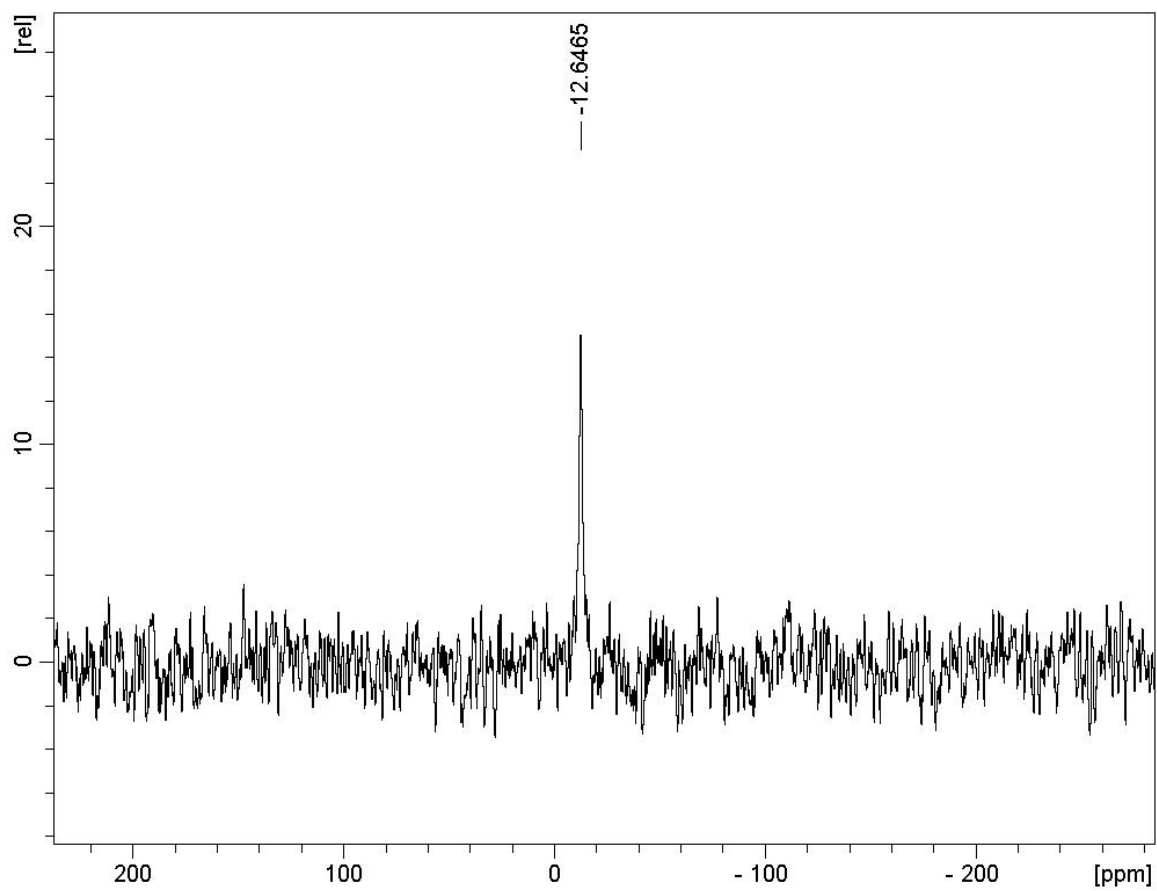
The single signal at -12.65 ppm indicates that the silicon carbon bond has survived the

reaction.

Figure S31: Solid-state ^{11}B NMR spectrum of COF-5 (model compound).
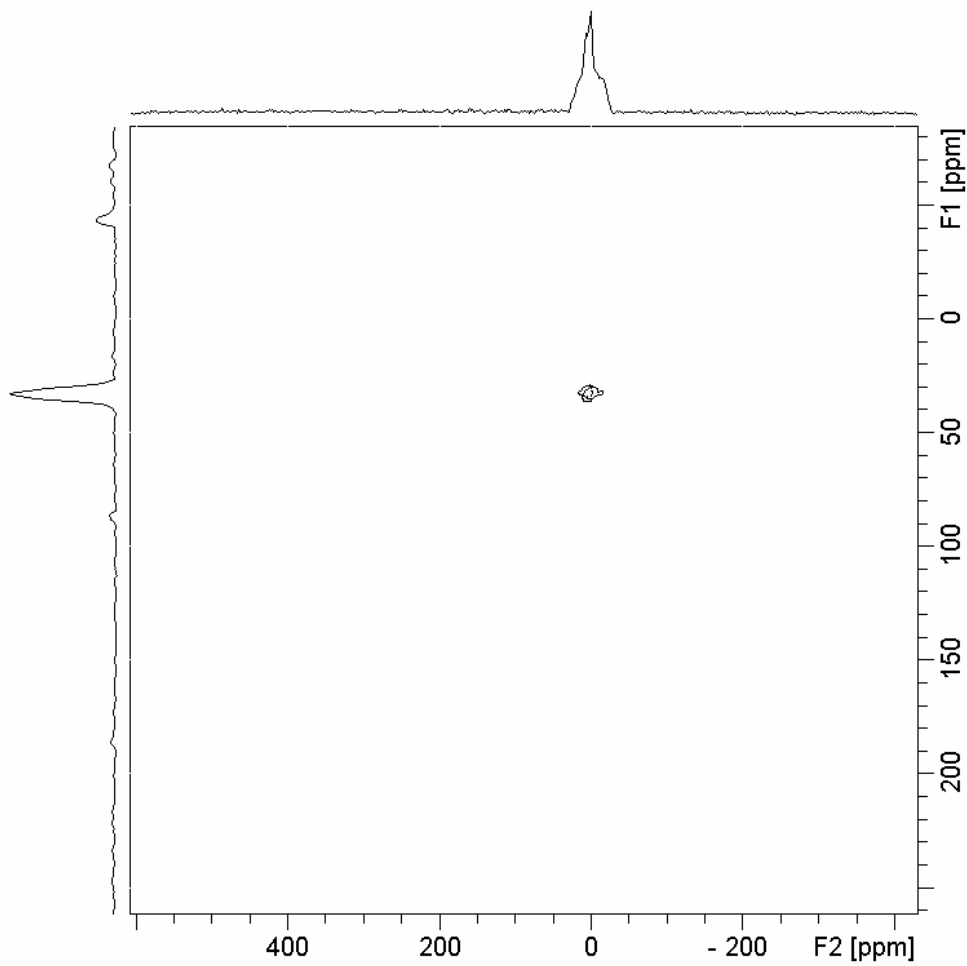
The single signal present shows only one type of boron species is present. The peak

shape is much different than that obtained for the starting material. This is the expected

result because the model compound should contain BO_2C_2 boronate esters which create a

different environment around the boron.

Figure S32: Solid-state ^{11}B NMR spectrum of COF-105.
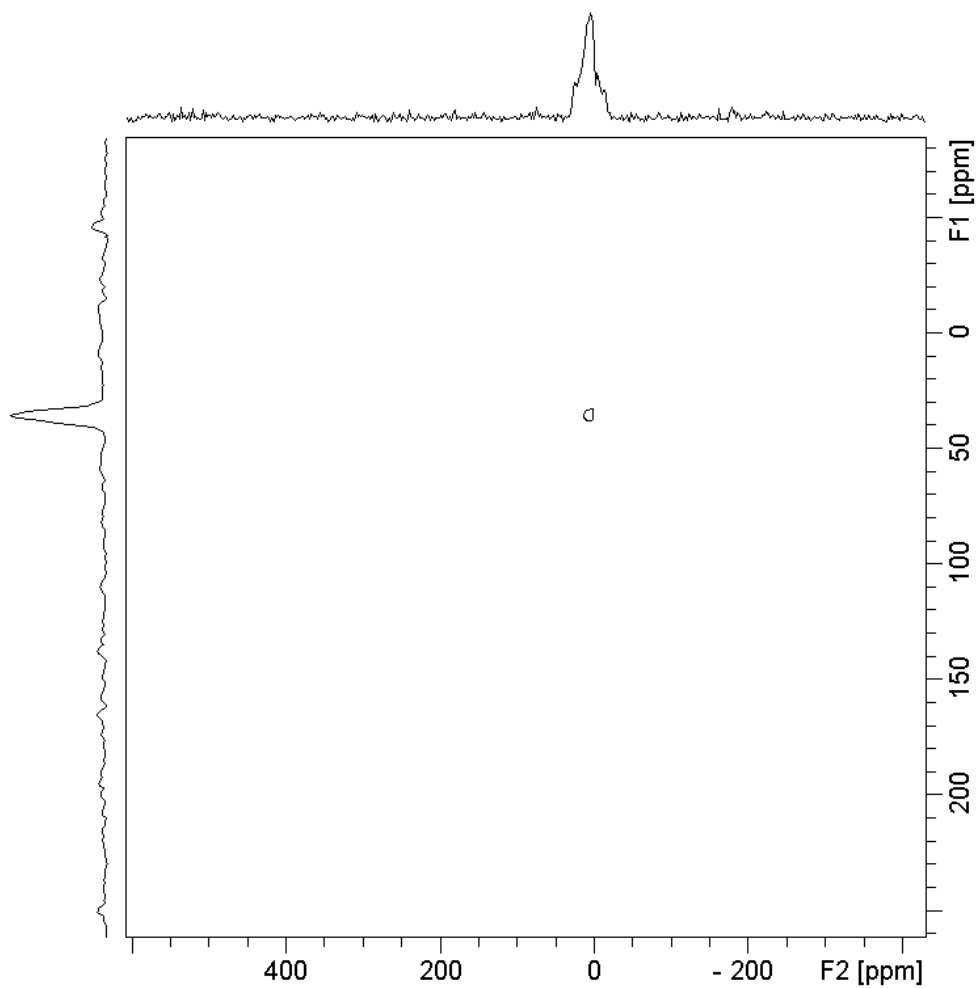
The single peak shows that the product is pure and contains only one type of boron atom. The distinctive peak shape is very different from the starting material and matches the peak shape obtained for the model compound (COF-5).

Figure S33: Stack plot comparing the ^{11}B NMR spectra of COF-105, COF-5 (model compound), and *tetra*(4-(dihydroxy)borylphenyl)silane.
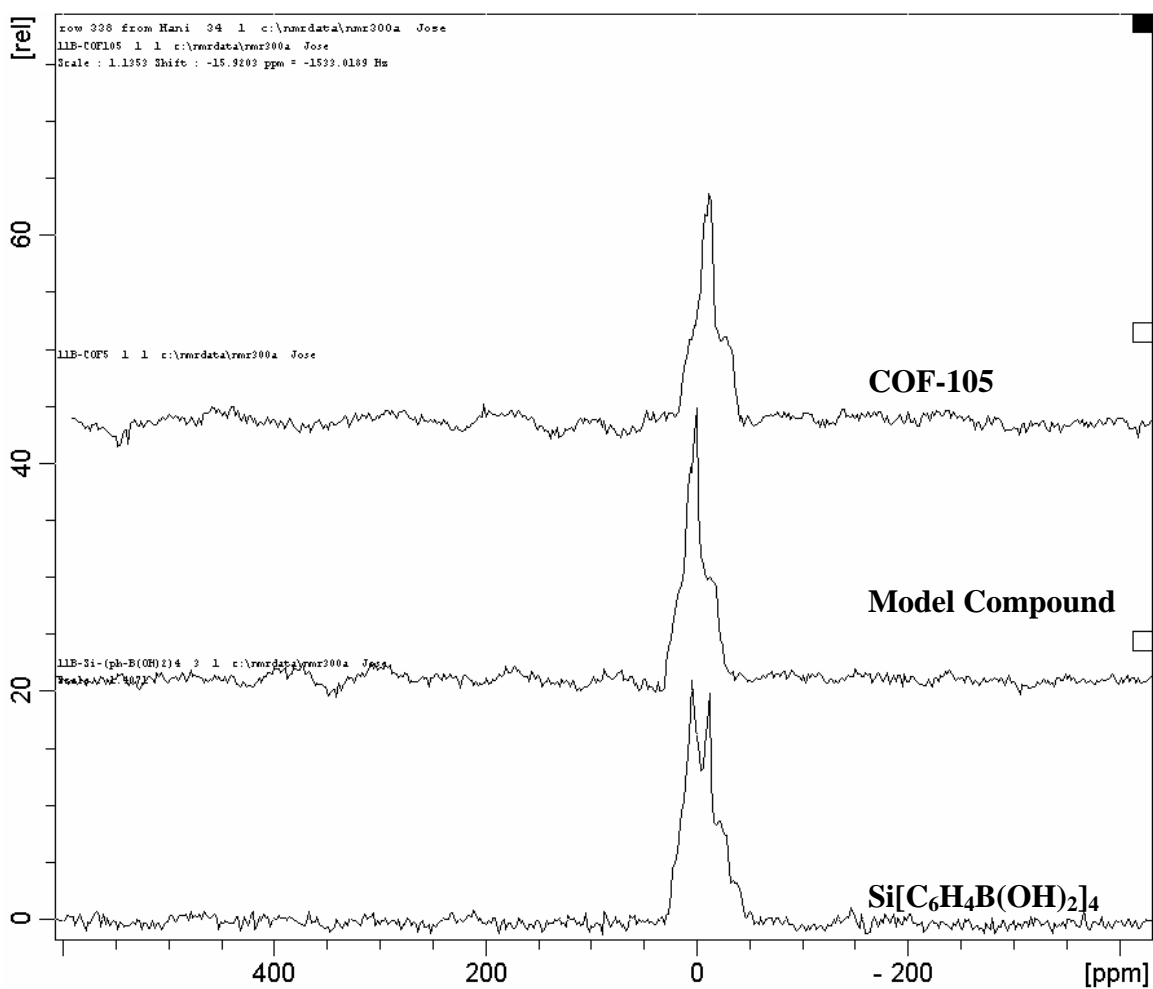
Figure S34: Solid-state ^{29}Si NMR spectrum for COF-105 showing the expected ^{29}Si signal for a tetraphenyl bonded Si nucleus at a chemical shift of -13.53 ppm. Note that spectrum of COF-105 contains only one resonance for the silicon nuclei exhibiting a chemical shift very similar to that of the tetra(4-(dihydroxy)borylphenyl)silane indicating the integrity of the tetrahedral block and the exclusion of any Si-containing impurities.
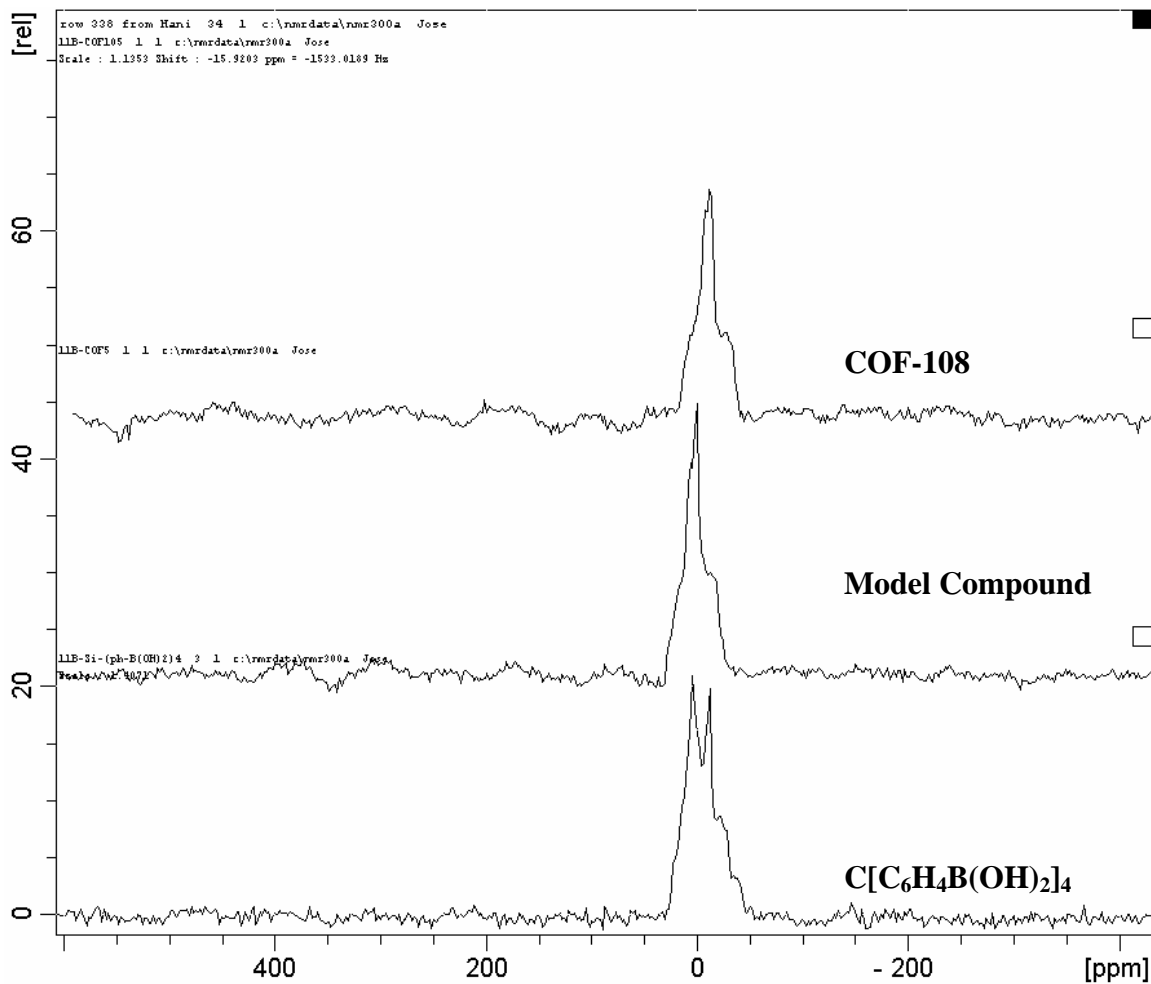
Figure S35: Solid-state ^{13}C NMR spectrum for COF-105. Note the resonances at 104.54 and 148.50 ppm indicate the incorporation of tetraphenylene molecule.
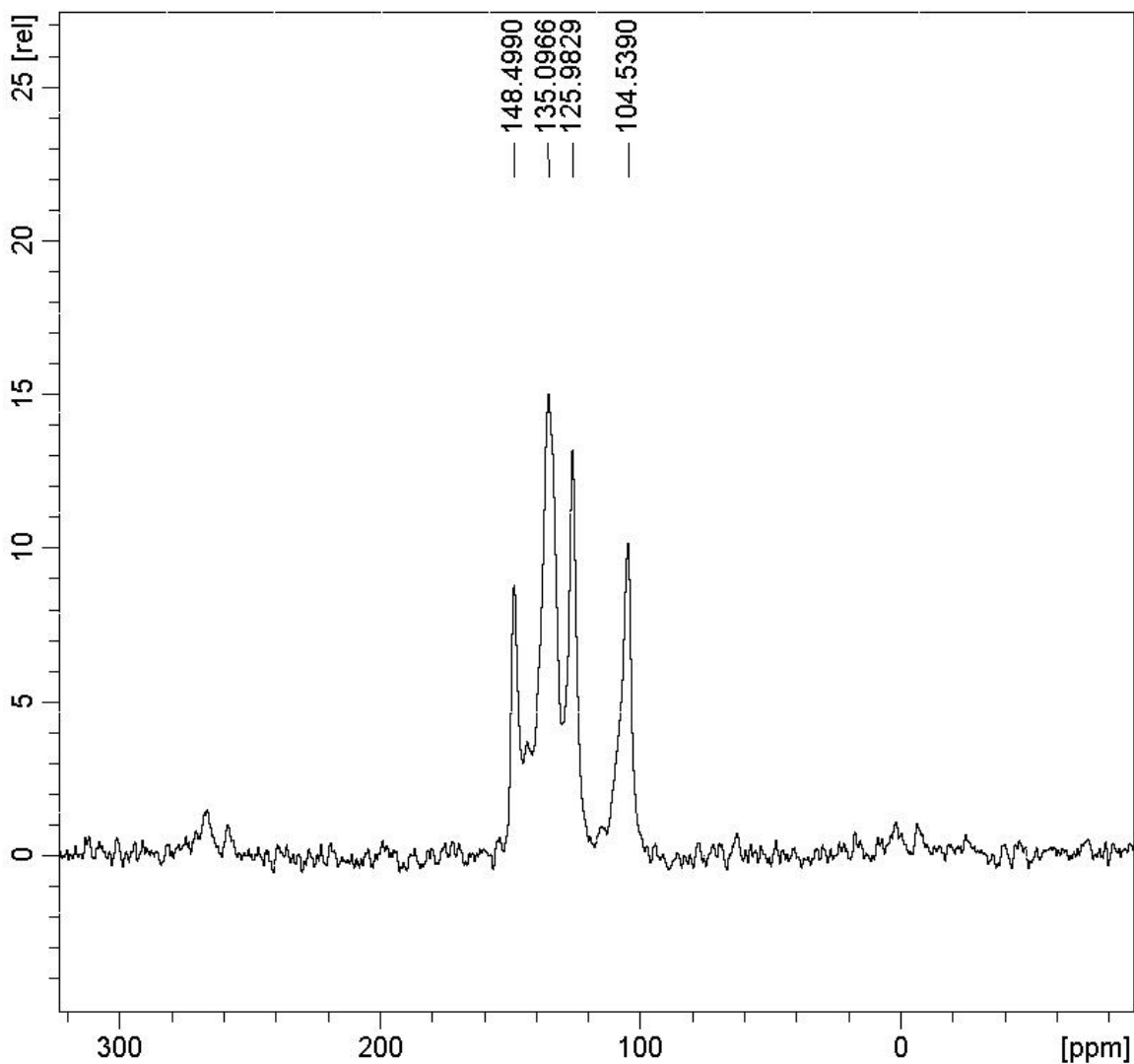
All the expected peaks from the starting material are present showing the survival of the building block. Peaks arising from incorporation of the HHTP are also present confirming the identity of the product. Some of the carbon signals are too close in chemical shift to be resolved.
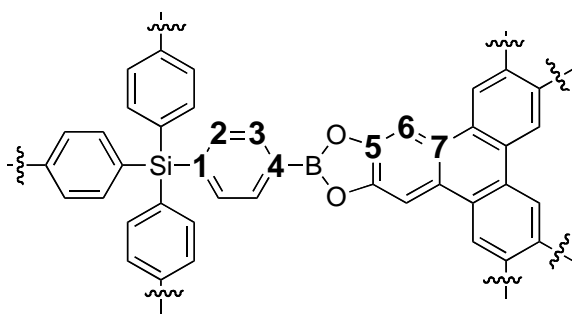
Carbon	Chemical Shift in ppm
1	148.50
2	135.10
3	135.10
4	135.10
5	148.50
6	104.66
7	125.98

Figure S36: Solid-state[11]B NMR spectrum of COF-108.
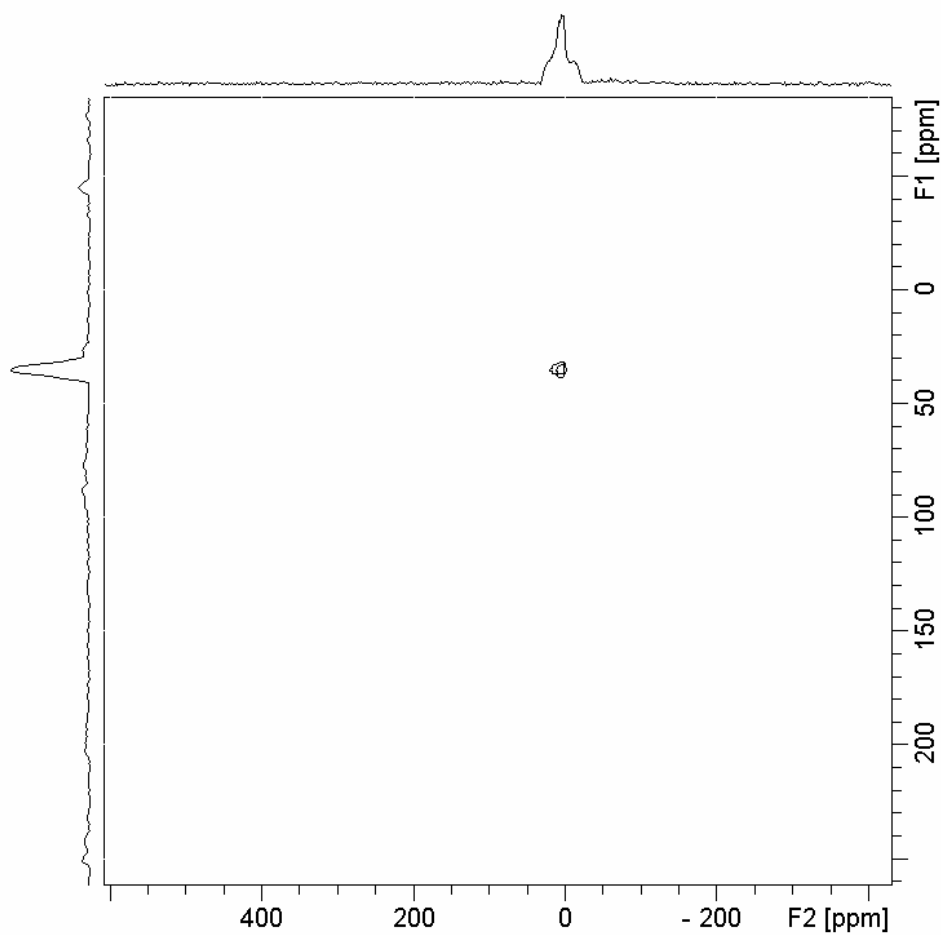
The single peak shows that the product is pure and contains only one type of boron atom.

The distinctive peak shape is very different from the starting material and matches the

peak shape obtained for the model compound (COF-5).

Figure S37: Stack plot comparing the solid-state ^{11}B NMR spectra of COF-108, COF-5, and *tetra*(4-(dihydroxy)borylphenyl)methane.

Figure S38: Solid-state ^{13}C NMR spectrum for COF-108. Note the resonances at 104.66 and 148.96 ppm indicate the incorporation of tetraphenylene molecule.
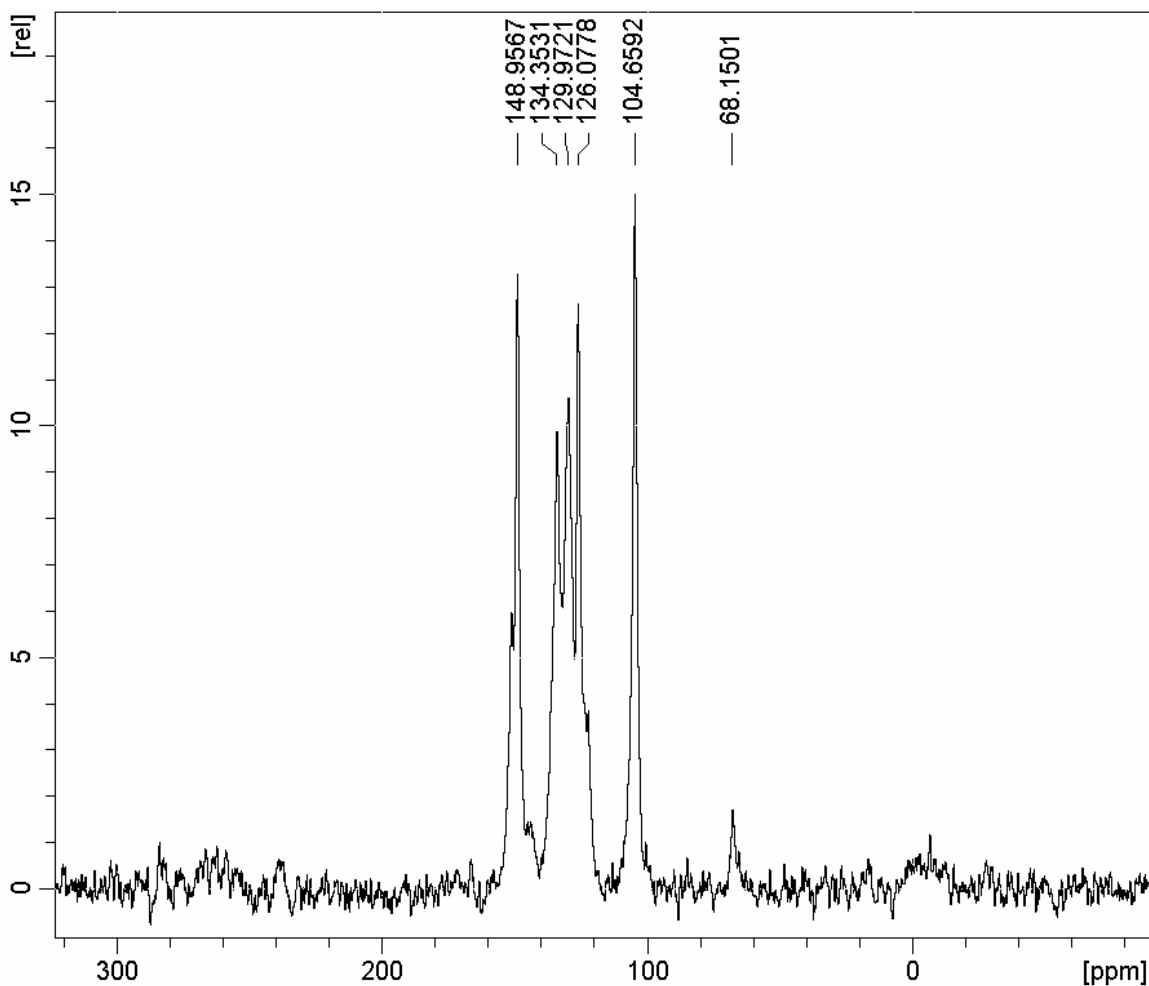
All the expected peaks from the starting material are present showing the survival of the building block. Peaks arising from incorporation of the HHTP are also present confirming the existence of the product.
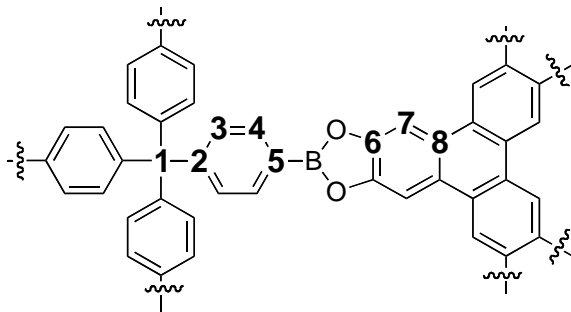
Carbon	Chemical Shift in ppm
1	68.15
2	148.96
3	135.10
4	134.35
5	129.97
6	148.96
7	104.66
8	125.98

Materials and Methods Section S6*: Scanning Electron Microscopy Imaging (SEM) of COF-102, COF-103, COF-105, and COF-108.*

In order to determine the purity of products, SEM was used to scan for all types of morphologies present in the samples. Multiple samples of each COF material were subjected to scrutinization under the SEM microscope. Only one type of morphology was found to exist for each compound confirming the purity of the materials produced. Samples of all 3-D COFs were prepared by dispersing the material onto a sticky carbon surface attached to a flat aluminum sample holder. The samples were then gold coated using a Hummer 6.2 Sputter at 60 millitorr of pressure in an argon atmosphere for 45 seconds while maintaining 15 mA of current. Samples were analyzed on a JOEL JSM-6700 Scanning Electron Microscope using both the SEI and LEI detectors with accelerating voltages ranging from 1kV to 15kV.

Figure S39: SEM image of COF-102 revealing a spherical morphology.

(a)
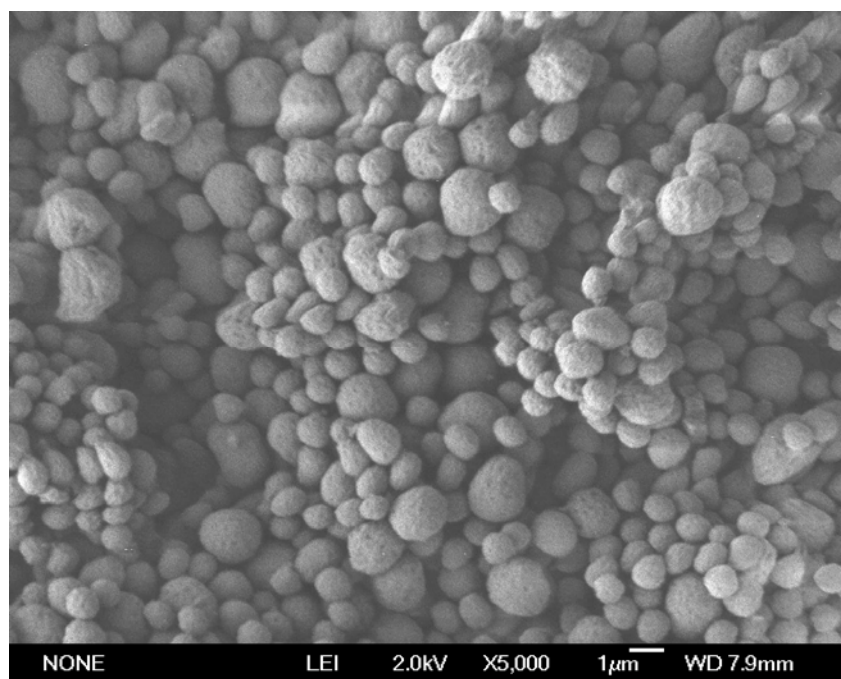
(b)
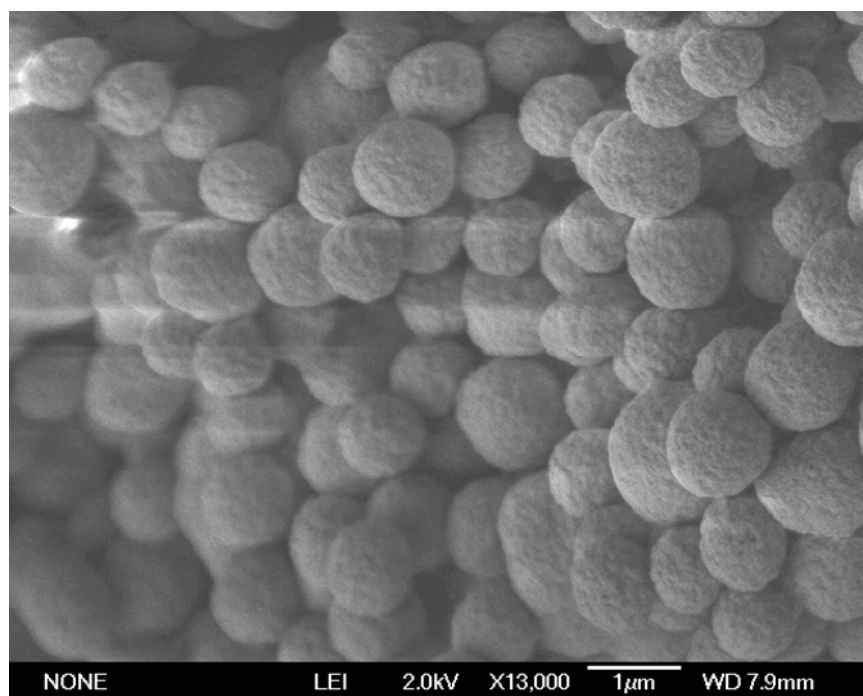
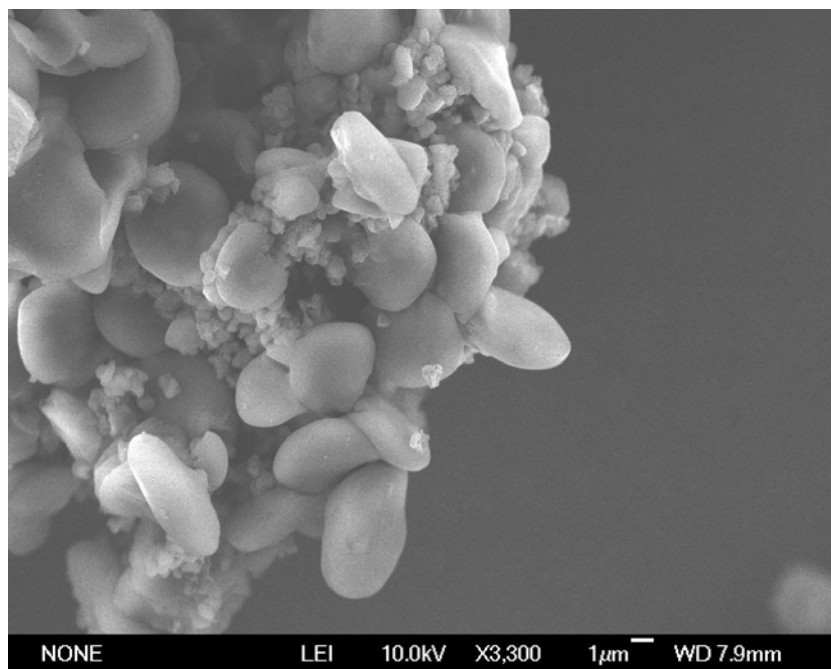**Figure S40**: SEM image of COF-103 revealing a spherical morphology.

(a)
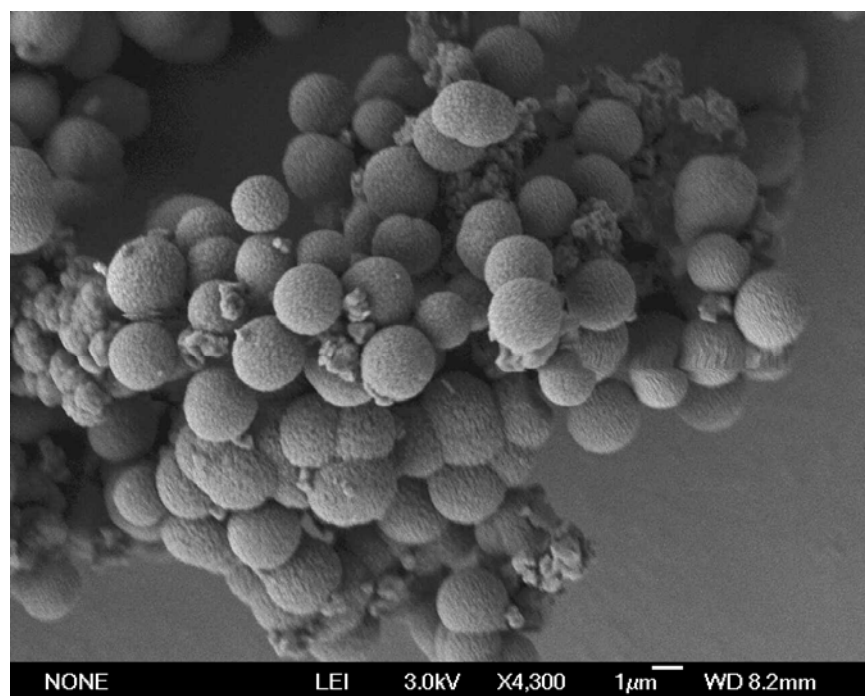
(b)
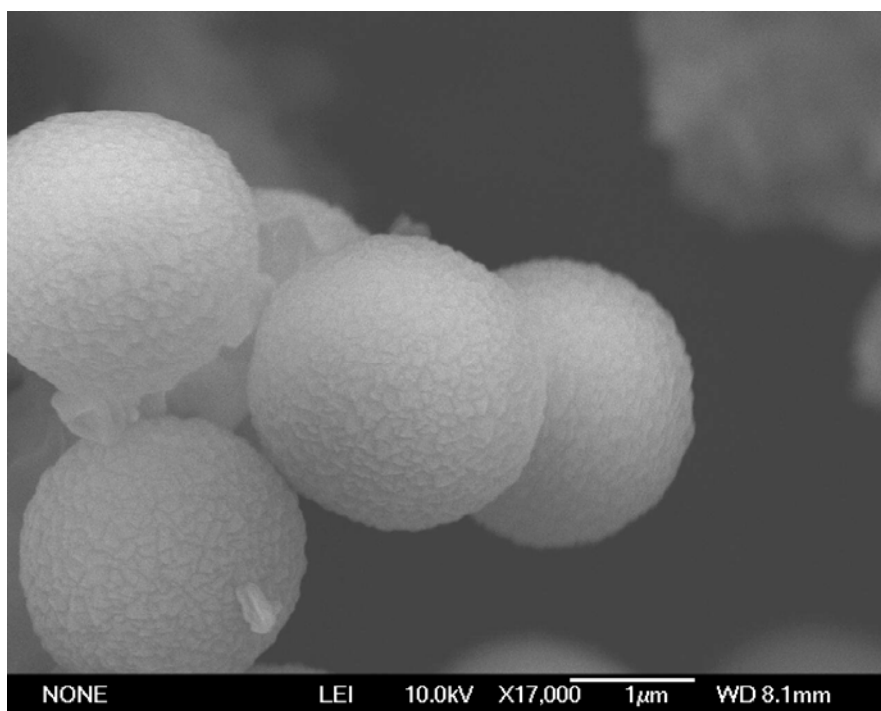
Figure S41: SEM image of COF-105 revealing platelet morphology.
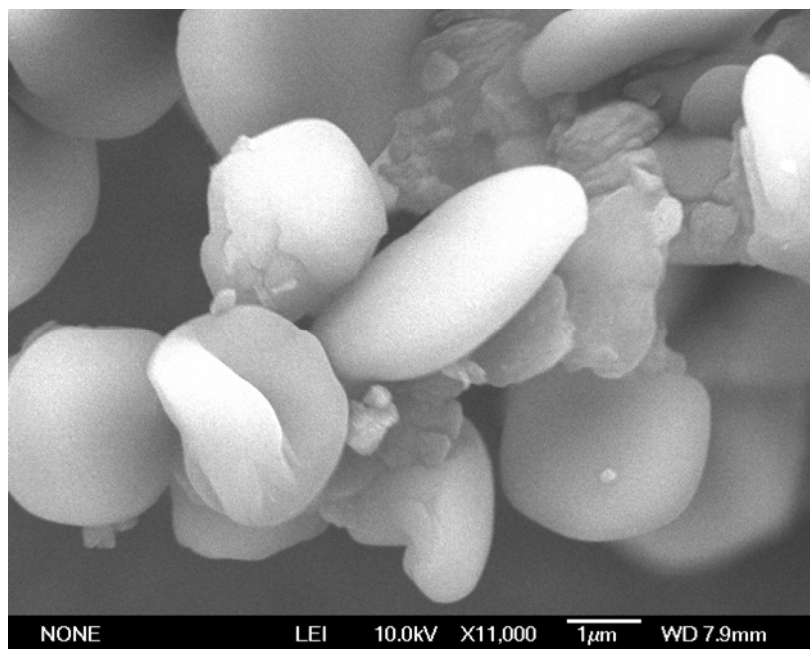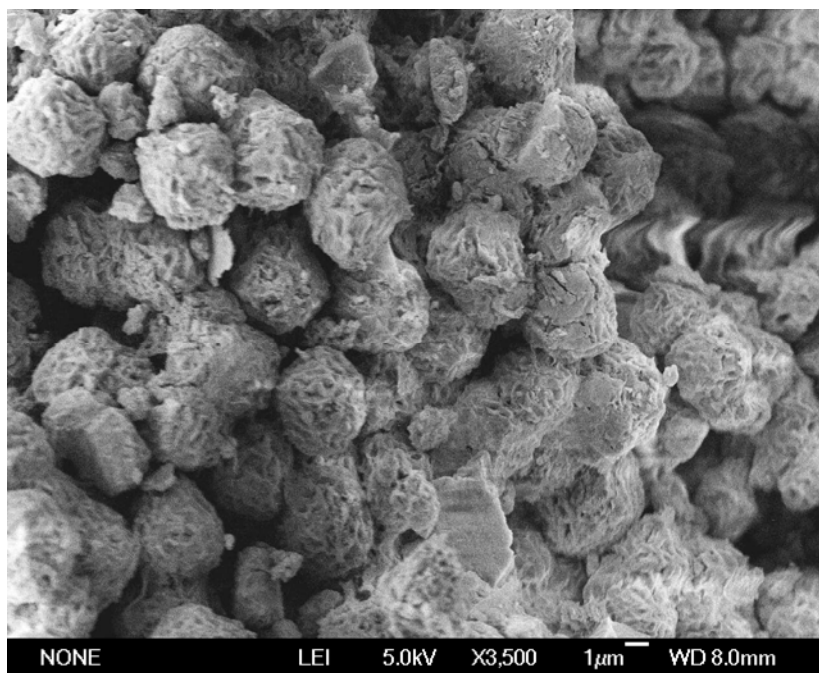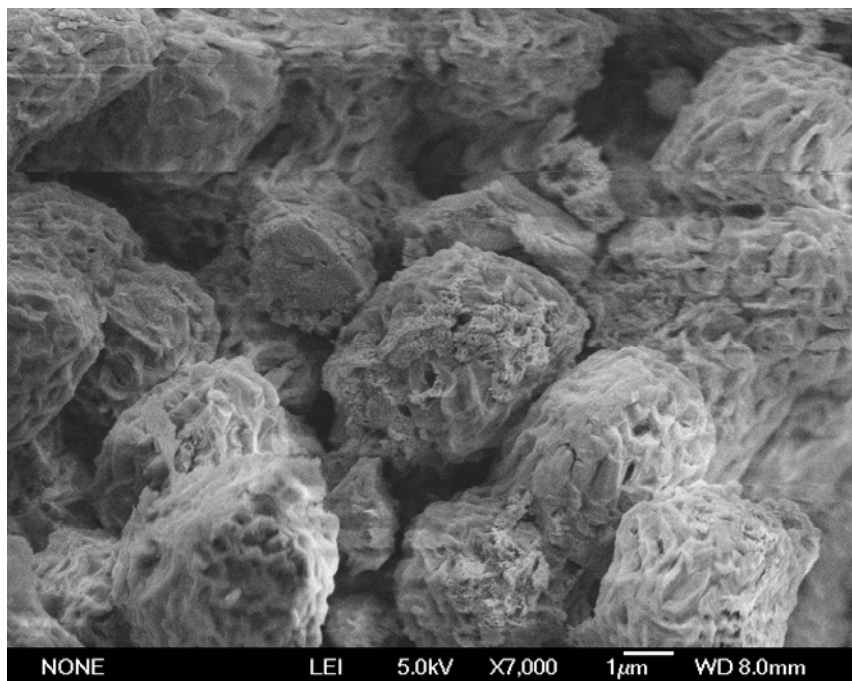
(a)

(b)

Figure S42: SEM image of COF-108 revealing a deformed spherical morphology.

(a)

(b)

Supplementary Section S7: *Thermogravimetric Analysis.*

All the COF materials were analyzed by TGA to determine the thermal stability of the materials produced as well as confirm that all guest have been removed. Samples were run on a TA Instruments Q-500 series thermal gravimetric analyzer with samples held in platinum pans under atmosphere of nitrogen. A 5 K/min ramp rate was used.

Figure S43: TGA trace for an activated sample of COF-102.
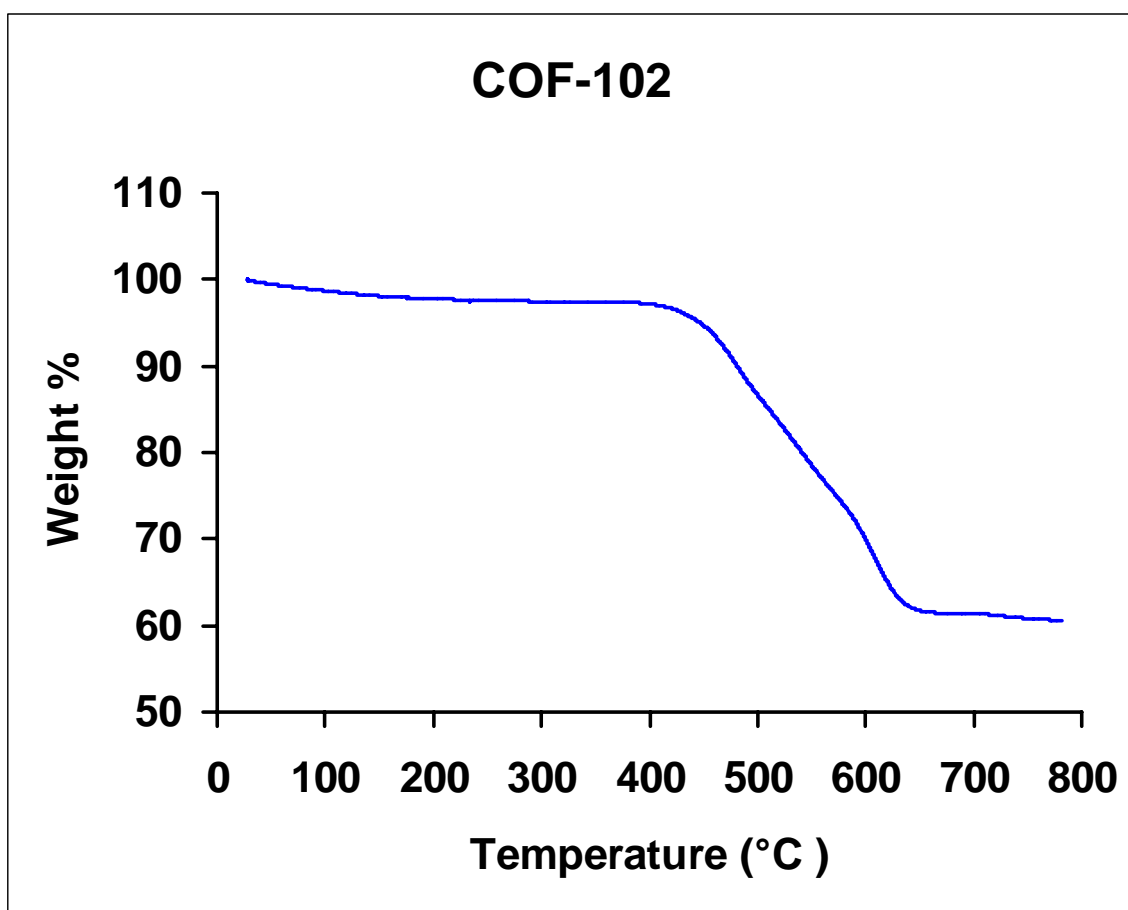
Figure S44: TGA trace for an activated sample of COF-103.
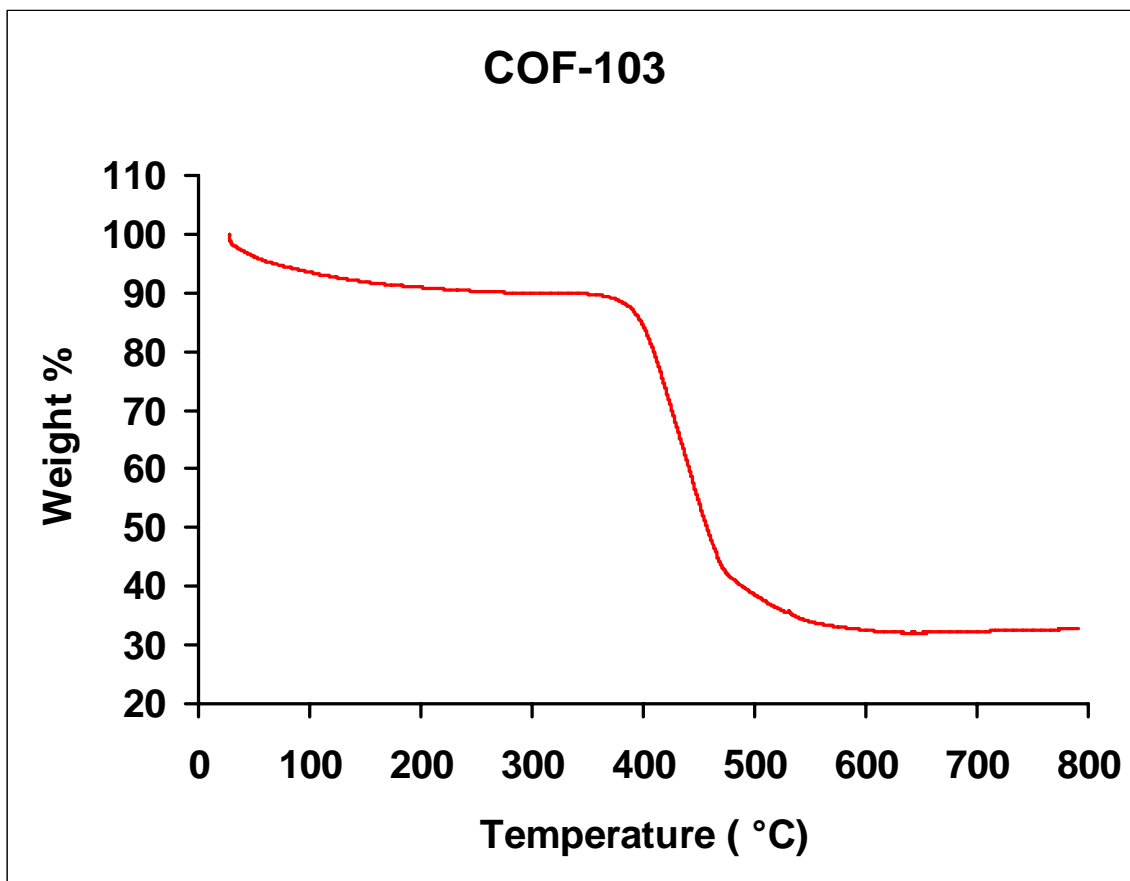

COF-103

Figure S45: TGA trace for an activated sample of COF-105.
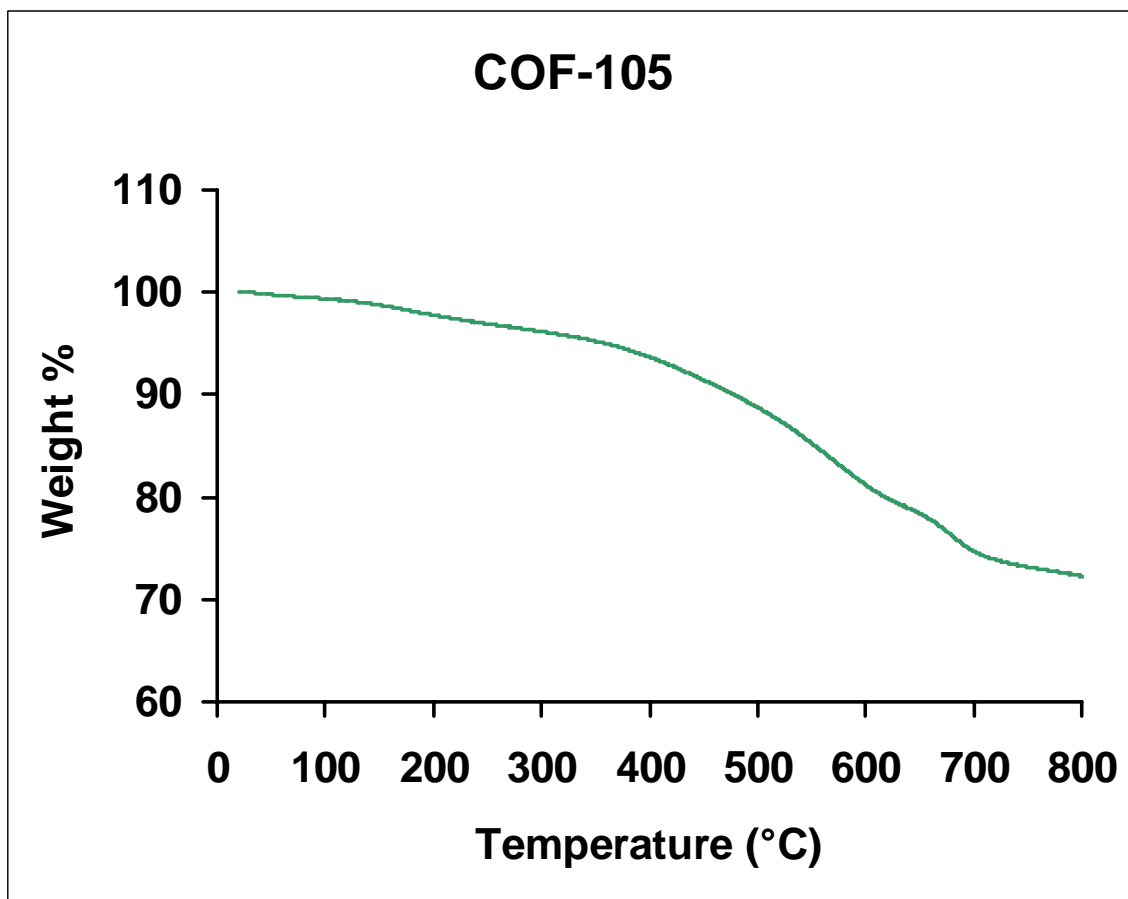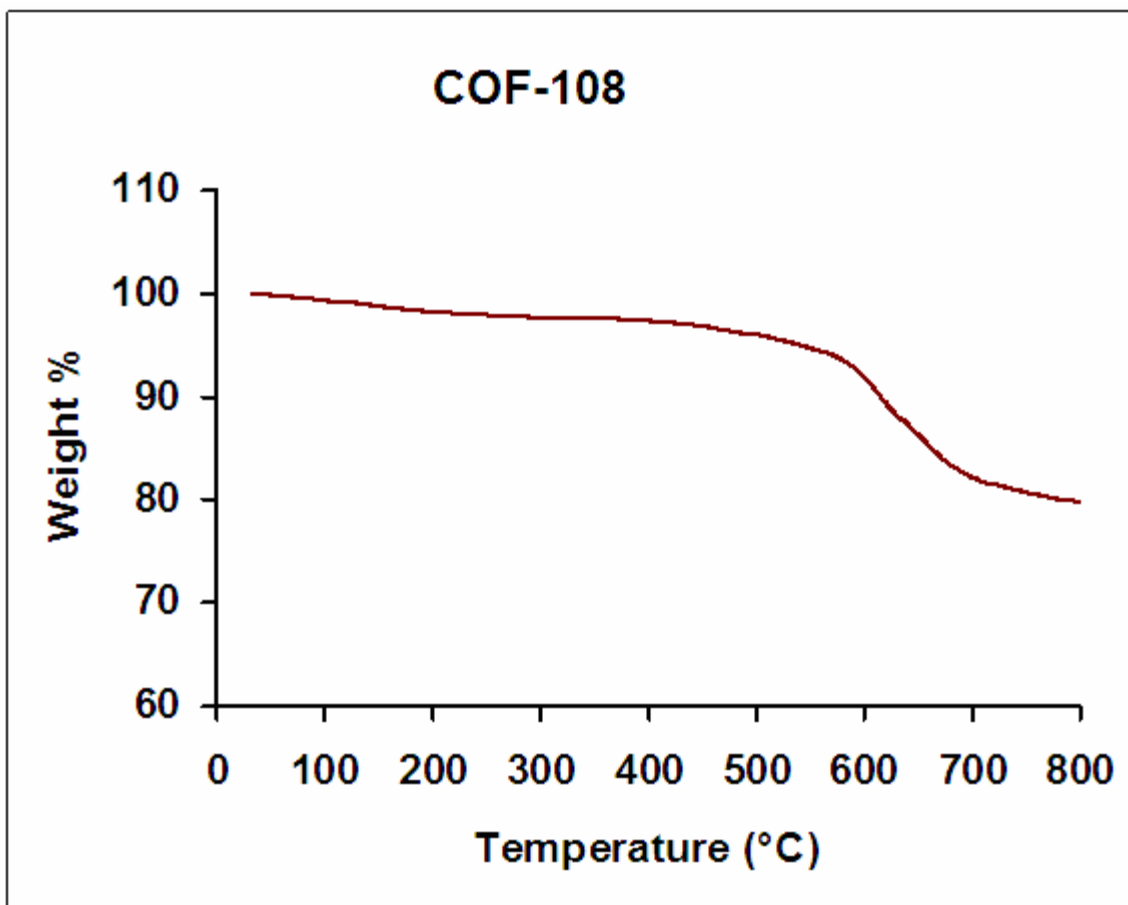
Figure S46: TGA trace for an activated sample of COF-108.

Supplementary Section S8: Low Pressure (0 – 760 mTorr) Argon Adsorption

Measurements for COF-102 and COF-103 at 87 K. The Pore Size Distribution of both

compounds was calculated from these adsorption isotherms by the Non-Local Density

Functional Theory (NLDFT) method using a cylindrical pore model (*13*).

Figure S47: Argon adsorption isotherm for COF-102 measured at 87 K and the Pore Size

Distribution (PSD) obtained from the NLDFT method. The filled circles are adsorption

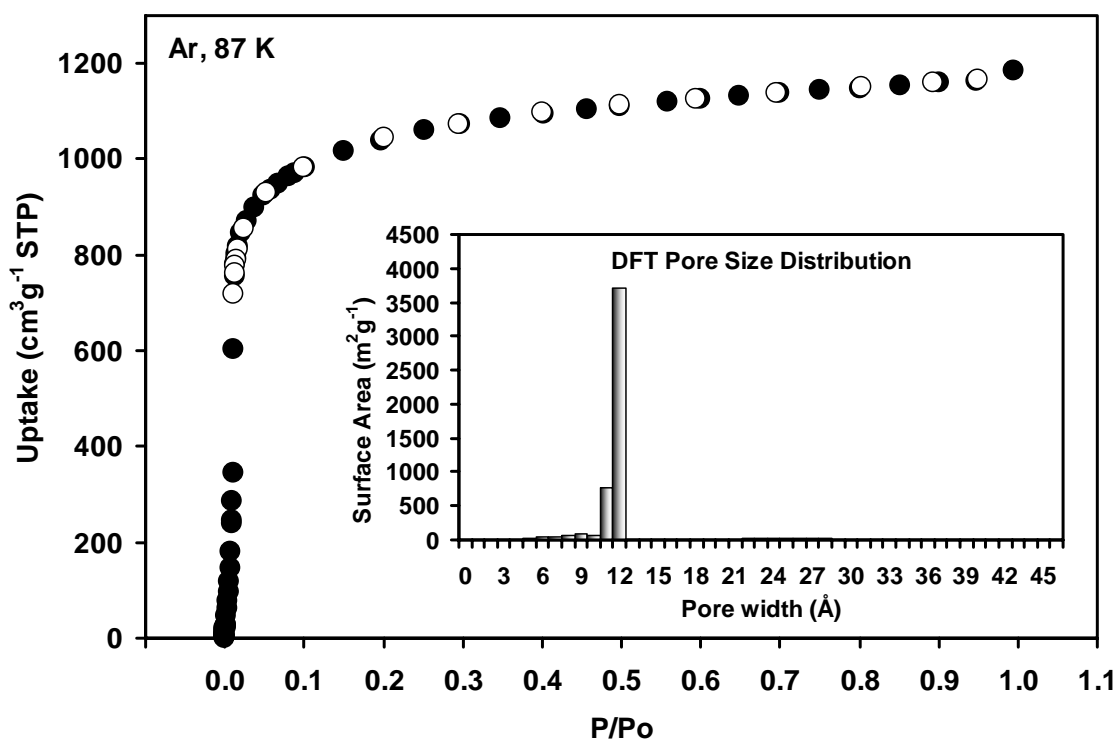points and the empty circles are desorption points.

Figure S48: Experimental Ar adsorption isotherm for COF-102 measured at 87 K is shown as filled circles. The calculated NLDFT isotherm is overlaid as open circles. Note that a fitting error of < 1 % indicates the validity of using this method for assessing the porosity of COF-102. The fitting error is indicated.
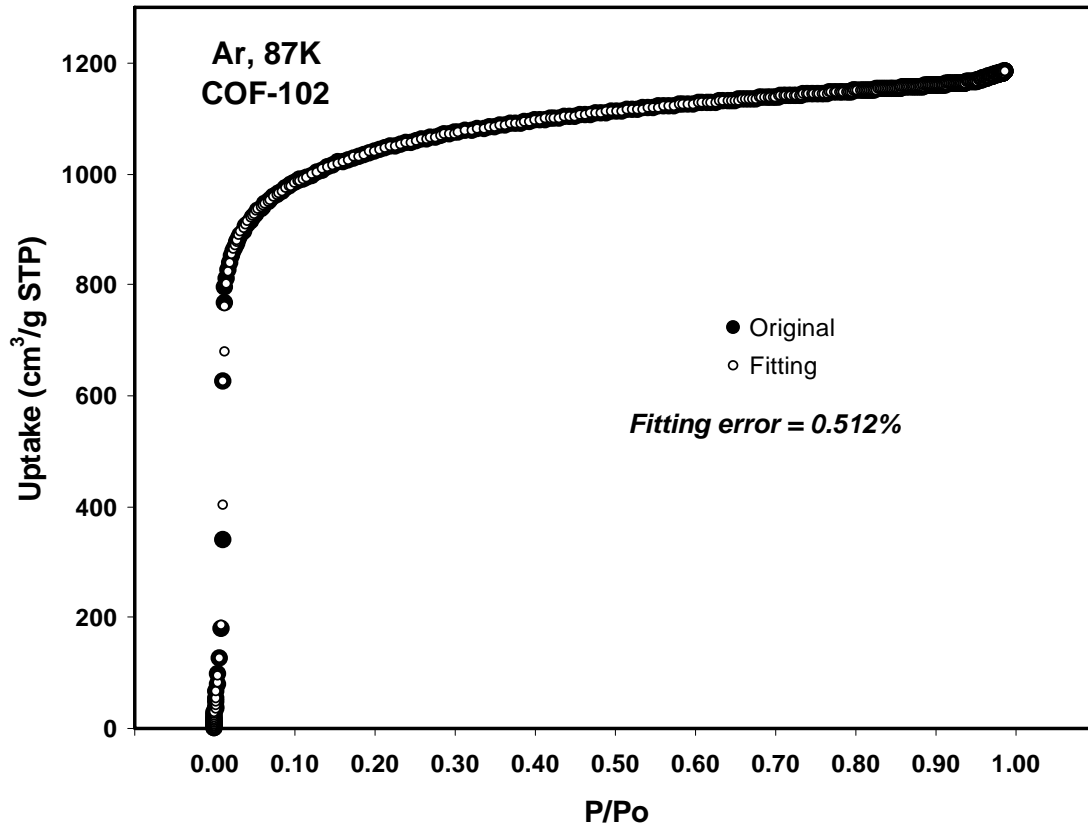
Figure S49: Langmuir plot for COF-102 calculated from the Ar adsorption isotherm at 87 K. The model was applied from P/P_o= 0.04-0.85. The correlation factor is indicated. (W = Weight of gas absorbed at a relative pressure P/P_o)
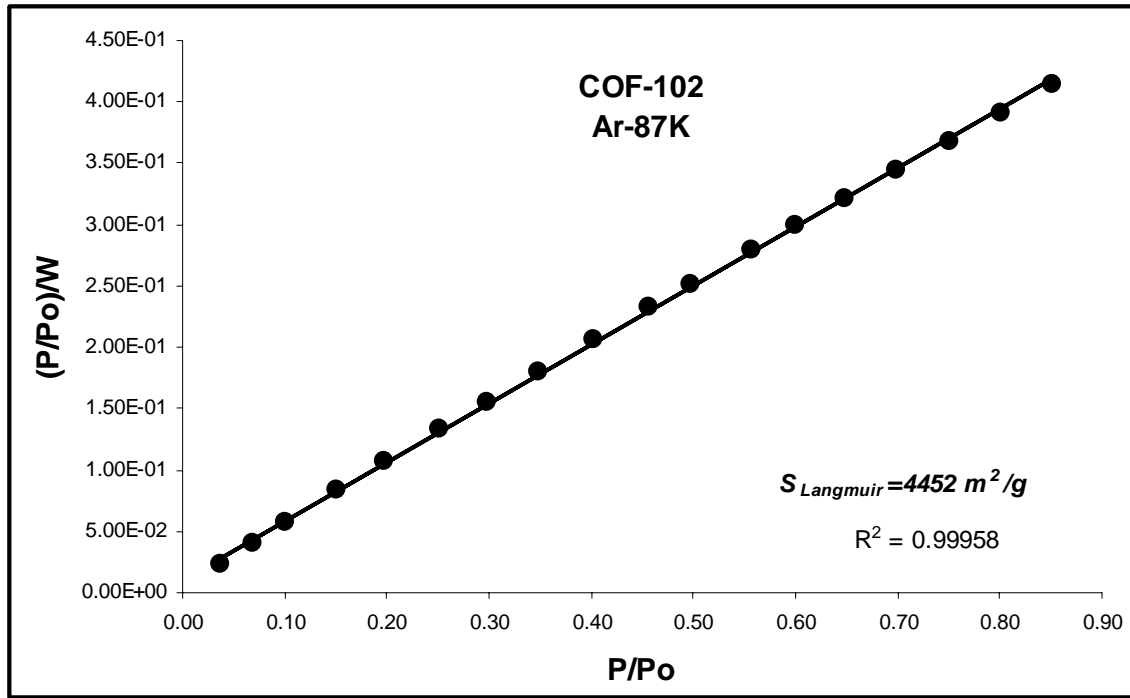
Figure S50: BET plot for COF-102 calculated from the Ar adsorption isotherm at 87 K. The model was applied from P/P_o= 0.01-0.10. The correlation factor is indicated. (W = Weight of gas absorbed at a relative pressure P/P_o).
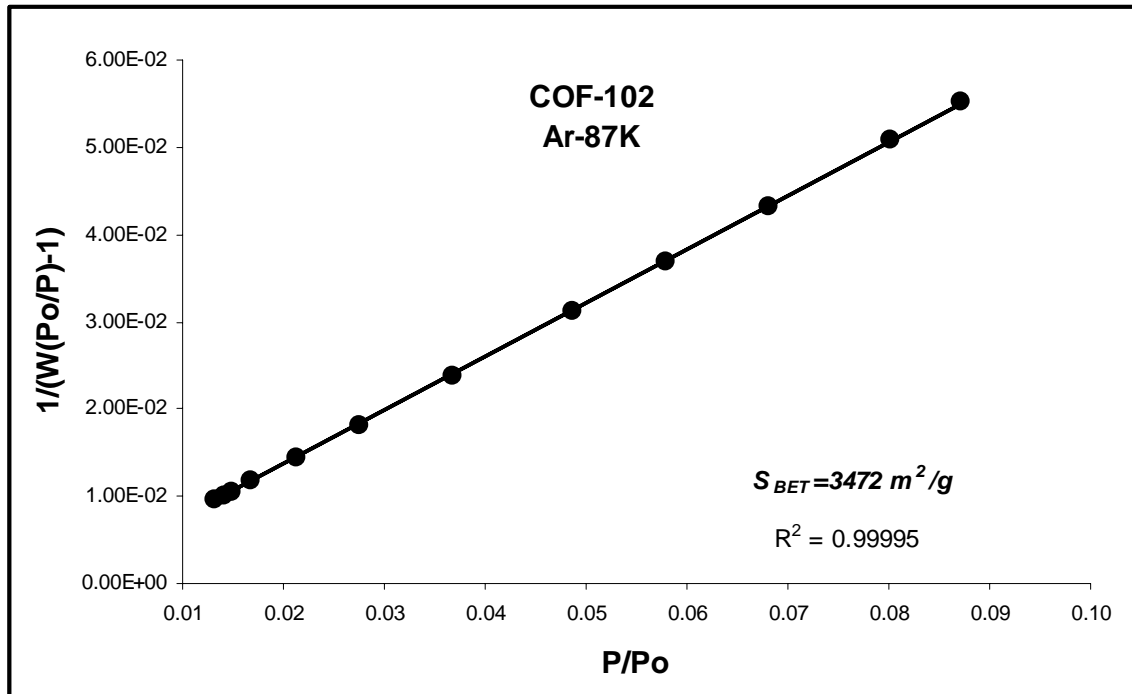
Figure S51: Argon adsorption isotherm for COF-103 measured at 87 K and the Pore Size Distribution (PSD) obtained from the NLDFT method. The filled circles are adsorption points and the empty circles are desorption points.
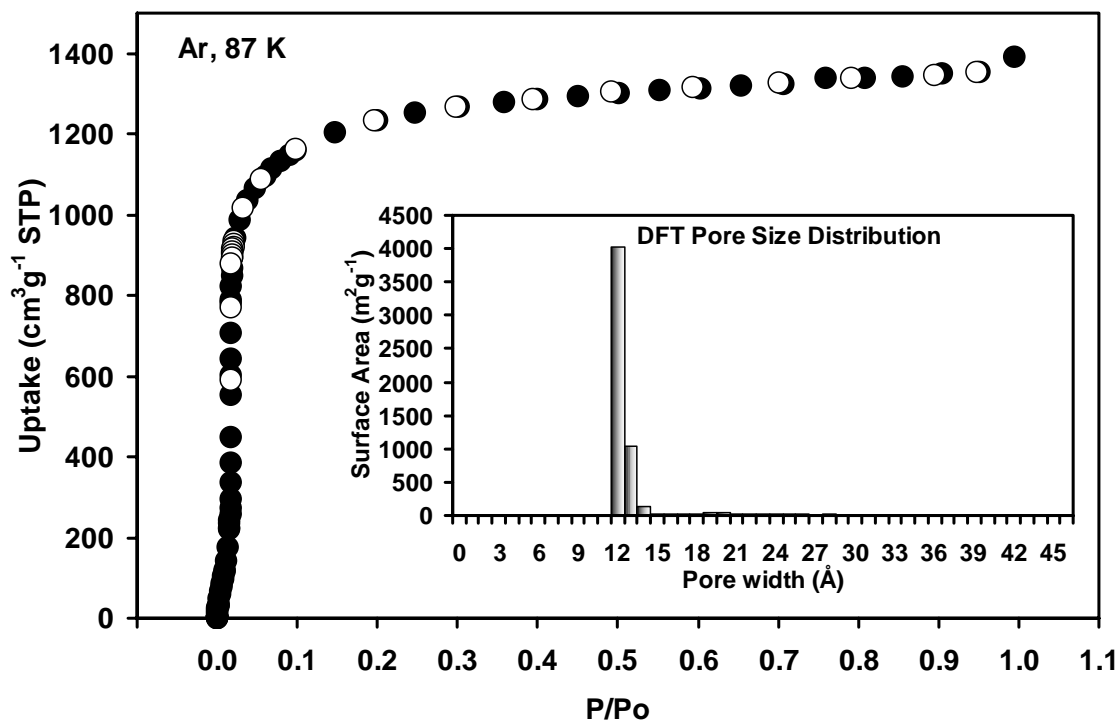
Figure S52: Experimental Ar adsorption isotherm for COF-103 measured at 87 K is showed as filled circles. The calculated NLDFT isotherm is overlaid as open circles. Note that a fitting error of < 1 % indicates the validity of using this method for assessing the porosity of COF-103. The fitting error is indicated.
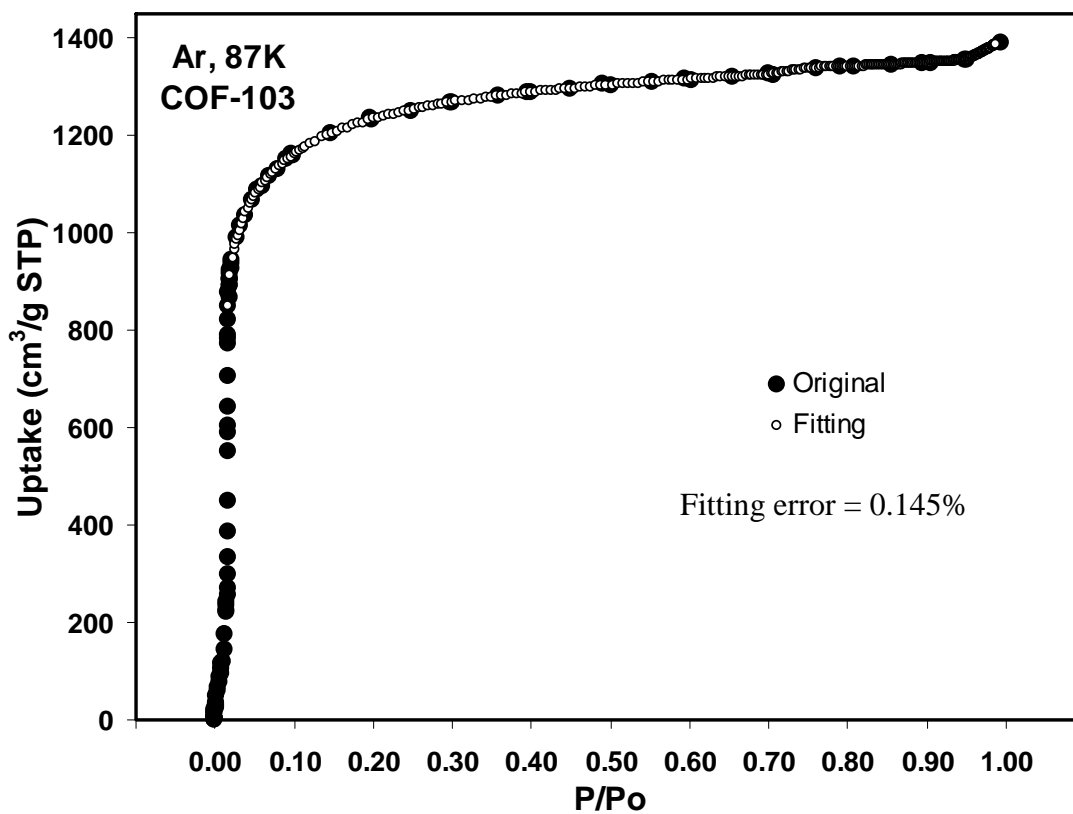
Figure S53: Langmuir plot for COF-103 calculated from the Ar adsorption isotherm at 87 K. The model was applied from P/P_o= 0.04-0.85. The correlation factor is indicated. (W = Weight of gas absorbed at a relative pressure P/P_o)
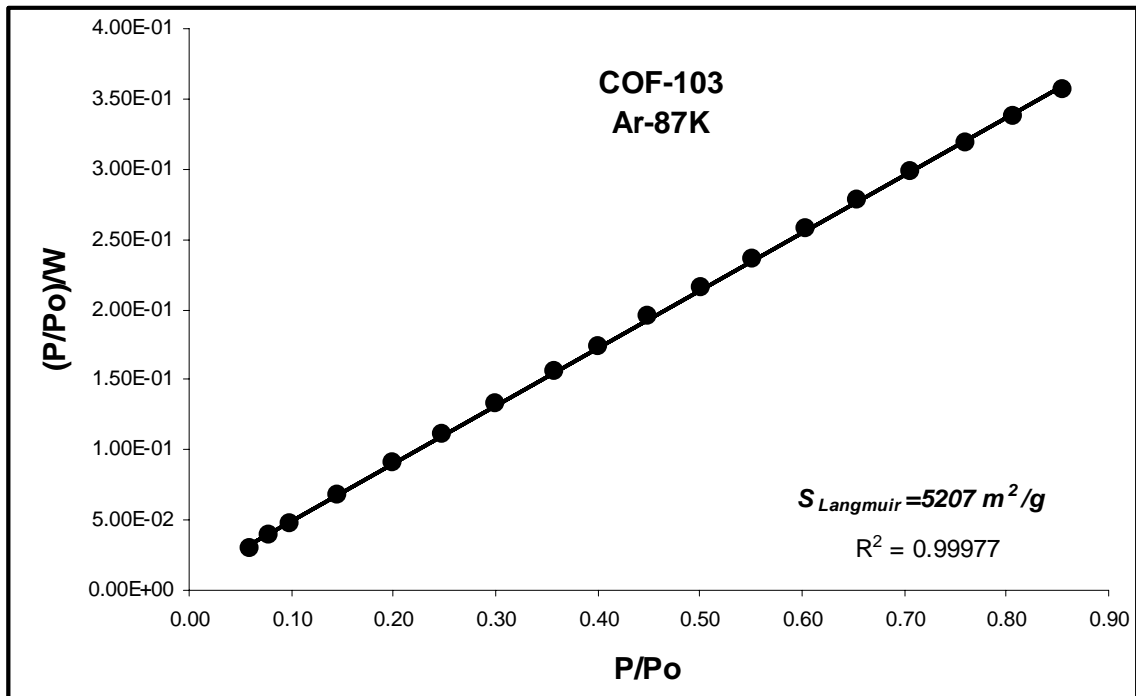
Figure S54: BET plot for COF-102 calculated from the Ar adsorption isotherm at 87 K. The model was applied from P/P_o= 0.01-0.10. The correlation factor is indicated. (W = Weight of gas absorbed at a relative pressure P/P_o).

Figure S55: Dubinin-Radushkevich plot used for pore volume estimation for COF-102 using argon gas. The Dubinin- Astakhov (DA) was applied and the same results were found (n=2).

Vp-COF-102
Ar-87K

$R^2 = 0.99867$

$Vp=1.345\ cm^3/g$
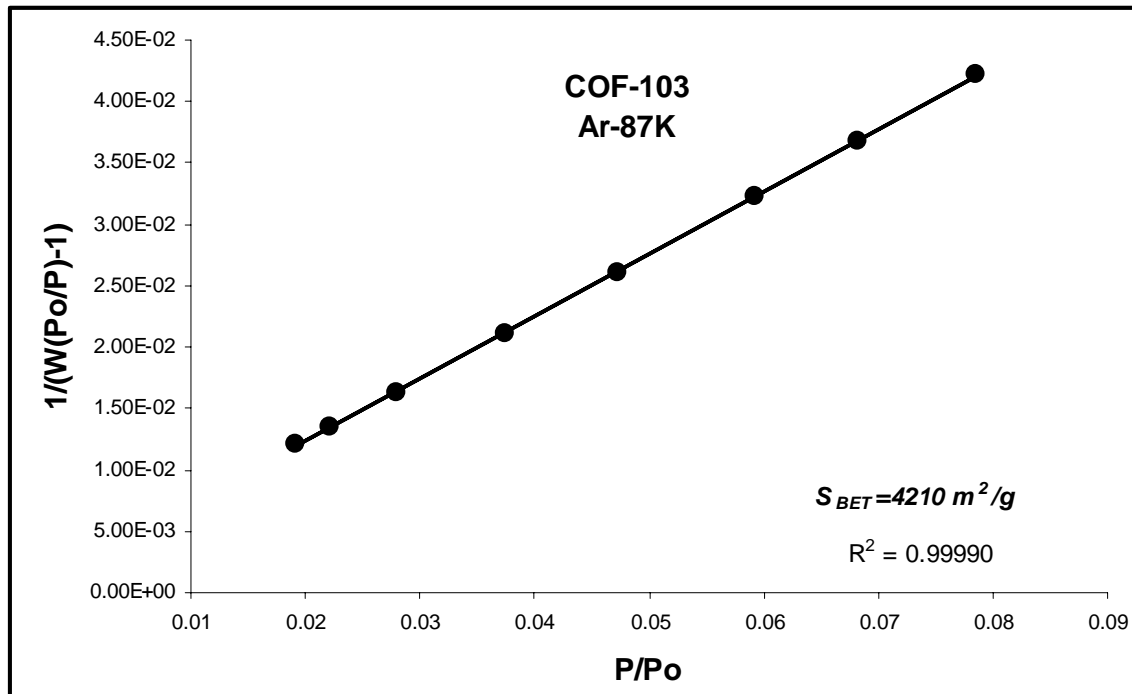
Weight absorbed (g)

$\log^n (Po/P),\ n=2$

Figure S56: Dubinin-Radushkevich plot used for pore volume estimation for COF-103 using argon gas. The Dubinin- Astakhov (DA) was applied and the same results were found (n=2).
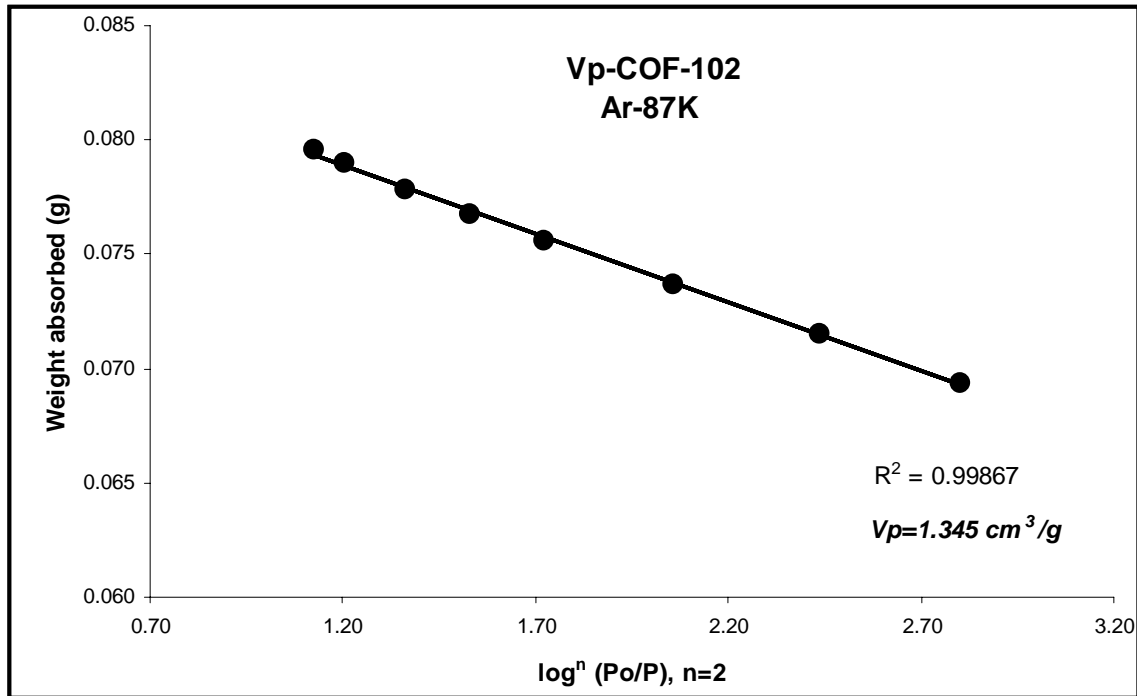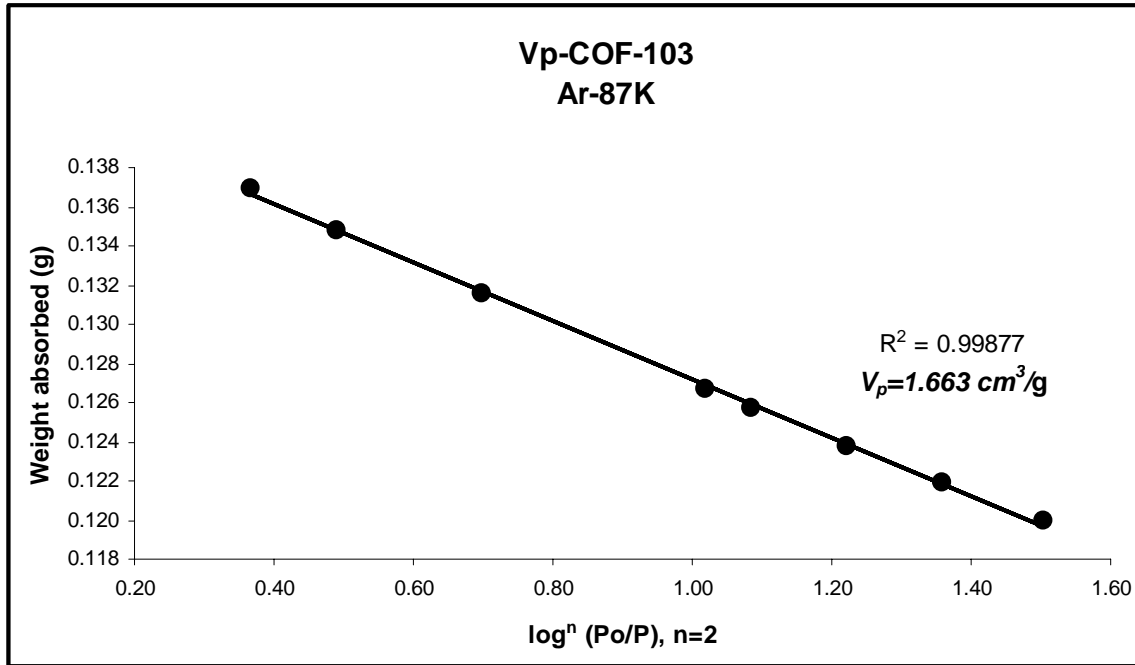

Vp-COF-103
Ar-87K

$R^2 = 0.99877$
$V_p = 1.663 \ cm^3/g$

Y-axis: **Weight absorbed (g)**

X-axis: $\mathbf{log^n \ (Po/P), \ n=2}$

References

1.   *Cerius*^{2} version 4.2 MatSci (2000 Molecular Simulations Inc., San Diego, CA, USA).

2.   O. Delgado-Friedrichs, M. O'Keeffe, O. M. Yaghi, *Acta Crystallogr. A*. **59**, 515 (2003).

3.   A. K. Rappe, C. J. Casewit, K. S. Colwell, W. A. Goddard-III, W. M. Skiff. *J. Am. Chem. Soc*. **114,** 10024 (1992).

4.   W. Kraus, G. Nolze, *J. Appl. Cryst.* **29**, 301 (1996).

5.   C. Dong, *J. Appl. Crystollogr.* **32**, 838 (1999)

6.   P.-E. Werner,.L. Eriksson, and M. Westdahl, *J. Appl. Crystollogr.* **18**, 367 (1985).

7.   J.-H. Fournier, T. Maris, J. D. Wuest, W. Guo, E. Galoppini, *J. Am. Chem. Soc.* **125**, 1002 (2003).

8.   A. P. Côté, A. I. Benin, N. W. Ockwig, M. O'Keeffe, A. J. Matzger, O. M. Yaghi, *Science* **310**, 1166 (2005).

9.   J. Schaefer, E. O. Stejskal, *J. Am. Chem. Soc*. **98**, 1031 (1976).

10.   A. E. Bennett, C. M. Rienstra, M. Auger, K. V. Lakshmi, and R. G. Griffin. *J. Chem. Phys*. **103**, 695 (1995).

11.   L. Frydman, J. S. Harwood, *J. Am. Chem. Soc.* **117**, 5367 (1995).

12.   A. Medik, J. S. Harwood, and L. Frydman, *J. Am. Chem. Soc.* **117**, 12779 (1995).

13.   K. Schumacher, P. I. Ravikovitch, A. Du Chesne, A. V. Neimark and Klaus K. Unger, *Langmuir*, **22**, 4648 (2000).